9 RELATIONSHIPS BETWEEN SEISMIC AND HYDROLOGICAL PROPERTIES

STEVEN R. PRIDE
Lawrence Berkeley National Laboratory, Berkeley, CA 94720

9.1 Introduction

Reflection seismology is capable of producing detailed three-dimensional images of the earth's interior at the resolution of a seismic wavelength. Such images are obtained by filtering and migrating the seismic data and give geometrical information about where in the earth the elastic moduli and mass densities change. However, information about which specific property has changed and by how much is not contained in the images. Hydrologists can use such migrated images to place geometrical constraints on their possible flow models, but must rely on well data to place constraints on the actual values of the hydrological properties.

With more effort, the seismic data may be inverted to yield the seismic velocity and attenuation structure within a region probed by the waves at a resolution of one or two wavelengths. However, the problem of further relating the seismic velocities and attenuation to hydrological properties such as permeability, porosity, and fluid type is still an ongoing research problem despite more than 50 years of effort. A computer program does not presently exist that can read in seismic data and output reliable information about permeability, porosity, or saturation.

Nonetheless, such hydrological properties can influence seismic properties, and much about the relationship is known. The theoretical framework for studying the connection is poroelasticity, which simultaneously provides the laws governing the hydrological response of a porous material caused by pumping and the seismic response caused by seismic sources. This chapter provides an up-to-date review of porous-media acoustics. It shows how seismic properties can change due to hydrological pumping and acts as a user's guide to the forward problem of predicting seismic wave speeds and attenuation from knowledge of porosity, saturation, and permeability. Similar recommendations for how to optimally perform the inverse problem and obtain hydrological properties from the seismic data are not yet available.

In Section 9.2, general expressions for the seismic wave speeds and attenuation in a porous material are obtained. The pedagogic exercise of obtaining the hydrological and seismic limiting cases of poroelasticity is also demonstrated. In Section 9.3, the definition and model of the dynamic permeability is obtained. In Section 9.4, definitions and models of the various poroelastic moduli are provided in the quasi-static limit where fluid-pressure is effectively uniform throughout each sample of the earth. In Section 9.5, these same moduli are modeled over the entire range of frequencies where the fluid-pressure equilibration on different spatial scales must be allowed for. Such wave-induced flow is responsible for attenuation and dispersion in porous materials and provides the possible link for obtaining permeability from seismic properties. Finally, in Section 9.6, the results of the chapter are discussed and interpreted with an eye toward understanding the possible connection between permeability and seismic properties.

9.2 Acoustics of isotropic porous materials

The governing equations for porous-media acoustics are generally credited to Biot (1956a,b, 1962), although Frenkel (1944) produced a similar set of equations.

Implicit in the standard form of Biot theory is that the porous material is uniform at "mesoscopic scales," which are those length scales lying between the "microscopic" grain scale and the "macroscopic" wavelength scale. As a compressional wave propagates through such a porous material, a fluid-pressure gradient is established between the peaks and troughs of the wave. The fluid tries to equilibrate by flowing from the peaks to the troughs. Such "macroscopic" flow is the only source of compressional-wave attenuation in standard Biot theory; however, this flow simply does not produce enough loss to explain the attenuation measured in both field work and most laboratory experiments involving geological materials.

To remedy this situation, a microscopic flow mechanism called "squirt" was proposed (Mavko and Nur, 1975, 1979; O'Connell and Budiansky, 1977; Dvorkin et al., 1995). Squirt flow is based on the fact that any broken grain contacts or microcracks in the grains are necessarily more compliant than the main part of the pore space. When a compressional wave squeezes the material, there is a larger fluid-pressure response in the microcracks than in the main pores, which results in a fluid flow from the microcracks to the main pore space. Such microscopic squirt flow can effectively explain ultrasonic attenuation data (frequencies near 1 MHz) obtained in the laboratory under ambient conditions. However, as will be explained in Section 9.5, squirt flow does not seem capable of explaining the measured attenuation in the seismic band of exploration frequencies (say, 10 Hz to several kHz).

One way to account for the attenuation in exploration work is if mesoscopic-scale heterogeneity is present. This heterogeneity may be due to patches of different immiscible fluids or to lithological variations (such as sand/shale mixtures, or pockets/fingers where the grains are less well cemented together, or the presence of joints/fractures within in a sedimentary host material). When a compressional wave squeezes a material having such mesoscopic heterogeneity, the effect is similar to squirt: the more compliant parts of the material respond with a greater fluid pressure than the stiffer portions. There results a mesoscopic flow of fluid that does seem capable of explaining the measured levels of attenuation in the seismic band as shown in Section 9.5. Early models of such mesoscopic flow were developed by White (1975) and White et al. (1975), while more recent models are those of Johnson (2001), Pride and Berryman (2003a,b), and Pride et al. (2003, 2004). An interesting aspect of the mesoscopic-loss mechanism is that it depends on the permeabilities of the materials present. Squirt loss, however, depends on h/R where h is the effective aperture of any microcracks in the grains of a rock and R is a characteristic grain radius. Squirt is only indirectly related to the permeability through the effective grain size R.

As shown in Section 9.5, both the micro and meso mechanisms result in the poroelastic moduli being complex and frequency dependent. The macro mechanism credited to Biot/Frenkel (wavelength scale equilibration) is normally modeled using real frequency-independent elastic moduli that are the focus of Section 9.4.

9.2.1 GOVERNING EQUATIONS OF POROUS MEDIA ACOUSTICS

Many authors, including Levy (1979), Burridge and Keller (1981), Pride et al. (1992) and Pride and Berryman (1998), have demonstrated that Biot's (1962) theory is the correct general model for porous-media acoustics. Assuming an $e^{-i\omega t}$ time dependence so that cumbersome time-convolution integrals (associated with the loss processes) are not explicitly present, Biot's (1962) equations controlling isotropic poroelastic response are

$$\nabla \cdot \boldsymbol{\tau}^D - \nabla P_c = -\omega^2(\rho \mathbf{u} + \rho_f \mathbf{w}) \tag{9.1}$$

$$-\nabla p_f = -\omega^2 \rho_f \mathbf{u} - i\omega \frac{\eta}{k(\omega)} \mathbf{w} \tag{9.2}$$

$$\boldsymbol{\tau}^D = G\left[\nabla \mathbf{u} + (\nabla \mathbf{u})^T - \frac{2}{3}\nabla \cdot \mathbf{u}\, \mathbf{I}\right] \tag{9.3}$$

$$-P_c = K_U \nabla \cdot \mathbf{u} + C \nabla \cdot \mathbf{w} \tag{9.4}$$

$$-p_f = C \nabla \cdot \mathbf{u} + M \nabla \cdot \mathbf{w}. \tag{9.5}$$

The various fields $\mathbf{u}$, $\mathbf{w}$, $\boldsymbol{\tau}^D$, P_c and p_f represent the average response in volumes that are much larger than the grains of the material but much smaller than the wavelengths. If $\overline{\mathbf{u}}_s$ is the average displacement of the solid grains throughout an averaging volume and $\overline{\mathbf{u}}_f$ the average displacement of the fluid in the pore space, then the displacement fields of the theory are $\mathbf{u} = \overline{\mathbf{u}}_s$ and $\mathbf{w} = \phi(\overline{\mathbf{u}}_f - \overline{\mathbf{u}}_s)$ where ϕ is the porosity of the averaging volume. When the area porosity defined on a slice of the porous material is equivalent to the volume porosity (for isotropic media, this can be considered exact in the limit of large averaging volumes), $-i\omega\mathbf{w}$ corresponds to the Darcy filtration velocity. The dilatation $\nabla \cdot \mathbf{u}$ can be shown (e.g., Pride and Berryman, 1998) to accurately represent the total volume dilatation of a sample of material (exactly so when the geometrical center of the grain space is coincident with the geometrical center of the pore space). The dilatation $\nabla \cdot \mathbf{w}$ corresponds to the accumulation or depletion of fluid in the sample and is often called the "increment of fluid content" (denoted $-\zeta$ by Biot). Let the tensor $\boldsymbol{\tau}$ represent the average stress tensor throughout the entire averaging volume (both solid and fluid). Upon separating this average total-stress tensor into isotropic and deviatoric portions $\boldsymbol{\tau} = -P_c \mathbf{I} + \boldsymbol{\tau}^D$ (where $\mathbf{I}$ is the identity tensor), the scalar $P_c = -\mathrm{tr}\{\boldsymbol{\tau}\}/3$ represents the average total pressure acting on a sample (the so-called "confining pressure"), while the tensor $\boldsymbol{\tau}^D$ represents the average shear stress. Last, p_f is the average fluid pressure throughout the pores of a sample.

Generally, the fields and moduli change with the size of the averaging volume. This size is ideally chosen so that the averaged fields correspond to those that a measuring device such as a geophone or geophone group records. In this manner, modeled fields and recorded data may be directly compared in the inverse problem. Alternatively, the size of the averaging volume implicitly corresponds to the size of the discretization element when these equations are solved numerically by finite difference, and is necessarily much smaller than the seismic wavelength. If laboratory experiments are performed to determine the moduli of the theory, the sample size corresponds to the averaging volume (and, therefore, discretization element) employed in the forward model (Pride and Berryman, 1998). Since

averaging volumes on the order of cubic meters (and even much larger) are commonly used in seismic forward modeling, one can properly say that no laboratory experiment has ever been performed that measures the moduli/coefficients at the scale required for the seismic forward modeling. Measurement of the moduli at the seismic length scale can only come indirectly from inversion of seismic data.

Equation (9.1) is the total balance of forces acting on each sample while Equation (9.2) is a generalized Darcy law and is itself a force balance on the fluid from a frame of reference fixed on the skeletal framework of grains. The apparent force $\omega^2\rho_f\mathbf{u}$ that acts along with $-\nabla p_f$ to drive the fluid flux $-i\omega\mathbf{w}$ is caused by wave-induced acceleration of this reference frame. The bulk density ρ of the rock is $\rho = (1-\phi)\rho_s + \phi\rho_f$ where ρ_f is the average density of the pore fluid and ρ_s the average density of the solid grains in a sample. The so-called "dynamic permeability" $k(\omega)$ is a complex frequency-dependent quantity such that at low-frequencies (to be precisely defined in Section 9.3.1) it is exactly the hydrological permeability k_o of a sample ($\lim_{\omega\to 0} k(\omega) = k_o$) while at high-enough frequencies it includes inertial effects associated with the relative fluid-solid movement. The viscosity of the pore fluid is η.

Equations (9.3)–(9.5) are the constitutive equations. Since linear wave propagation is being assumed, the displacements can always be considered small. As such, we have forgone placing a differential "d" in front of the various stresses and strains appearing in Equations (9.3)–(9.5). However, these constitutive equations are obtained by differentiating a strain-energy function and, as such, should always be thought of as differential equations (changes in strain related to changes in stress). Models for the three poroelastic incompressibilities K_U, C, M and for the shear modulus G are the focus of Sections 9.4 (quasi-static) and 9.5 (frequency dependent).

9.2.2 SEISMIC WAVE PROPERTIES

The seismic wave speeds, attenuation, and fluid-pressure diffusivity implicitly contained in Equations (9.1)–(9.5) are now obtained. These results are independent of whether the coefficients k, K_U, C, M, and G are complex and frequency dependent. The low-frequency limit of Equations (9.1)–(9.5) is also shown to yield both the laws of hydrology and seismology.

To obtain these results, one need only consider a homogeneous porous continuum and insert the stress/strain relations into the force balances to obtain

$$\left[(K_U + G/3)\nabla\nabla + (G\nabla^2 + \omega^2\rho)\mathbf{I}\right]\cdot\mathbf{u} + \left[C\nabla\nabla + \omega^2\rho_f\mathbf{I}\right]\cdot\mathbf{w} = 0 \quad (9.6)$$

$$\left[C\nabla\nabla + +\omega^2\rho_f\mathbf{I}\right]\cdot\mathbf{u} + \left[M\nabla\nabla + \omega^2\tilde{\rho}\mathbf{I}\right]\cdot\mathbf{w} = 0 \quad (9.7)$$

where $\mathbf{I}$ is again the identity tensor and where the relative-flow resistance in the Darcy law has been written as if it were an inertial property

$$\tilde{\rho}(\omega) = \frac{i}{\omega}\frac{\eta}{k(\omega)}. \quad (9.8)$$

We consider a plane wave that, by definition, has a material response of the form

$$\mathbf{u} = U\exp(i\mathbf{k}\cdot\mathbf{r})\hat{\mathbf{u}} \quad \text{and} \quad \mathbf{w} = W\exp(i\mathbf{k}\cdot\mathbf{r})\hat{\mathbf{w}}. \quad (9.9)$$

Here, $\hat{\mathbf{u}}$ and $\hat{\mathbf{w}}$ are unit vectors defining the polarization of the response, while $\mathbf{k}$ is the wave vector that we write in the form

$$\mathbf{k} = \omega s(\omega)\hat{\mathbf{k}}, \tag{9.10}$$

where $s(\omega)$ is the complex slowness (to be determined) and $\hat{\mathbf{k}}$ is a unit vector in the direction of propagation.

The quantities of interest are the phase velocity v and attenuation coefficient a (units of inverse length) for the various wave types that are related to the complex slowness as

$$v(\omega) = 1/\mathrm{Re}\{s(\omega)\} \quad \text{and} \quad a(\omega) = \omega \mathrm{Im}\{s(\omega)\}. \tag{9.11}$$

Taking $\hat{\mathbf{k}}$ to be in the x direction, the plane-wave spatial response is then of the form $e^{-a(\omega)x}e^{i\omega x/v(\omega)}$ and a is seen to control the exponential decay of the wave amplitude with distance x propagated. It is sometimes convenient to use the inverse of the quality factor Q (dimensionless) given by

$$Q^{-1}(\omega) = \frac{2a(\omega)v(\omega)}{\omega} = 2\frac{\mathrm{Im}\{s(\omega)\}}{\mathrm{Re}\{s(\omega)\}} \tag{9.12}$$

as the measure of attenuation. By definition, Q^{-1} represents the energy lost in a wave period divided by the average stored strain energy (and divided by 4π).

Putting the plane-wave response into Equations (9.6) and (9.7) gives

$$\begin{bmatrix} (K_U + G/3)s^2(\hat{\mathbf{k}}\cdot\hat{\mathbf{u}})\hat{\mathbf{k}} - (\rho - Gs^2)\hat{\mathbf{u}} & Cs^2(\hat{\mathbf{k}}\cdot\hat{\mathbf{w}})\hat{\mathbf{k}} - \rho_f\hat{\mathbf{w}} \\ Cs^2(\hat{\mathbf{k}}\cdot\hat{\mathbf{u}})\hat{\mathbf{k}} - \rho_f\hat{\mathbf{u}} & Ms^2(\hat{\mathbf{k}}\cdot\hat{\mathbf{w}})\hat{\mathbf{k}} - \tilde{\rho}\hat{\mathbf{w}} \end{bmatrix} \begin{bmatrix} U \\ W \end{bmatrix} = 0. \tag{9.13}$$

By definition, a transverse wave has a material response perpendicular to the wave direction ($\hat{\mathbf{k}}\cdot\hat{\mathbf{u}} = \hat{\mathbf{k}}\cdot\hat{\mathbf{w}} = 0$) while a longtitudinal wave has a material response parallel with the wave direction ($\hat{\mathbf{k}}\cdot\hat{\mathbf{u}} = \hat{\mathbf{k}}\cdot\hat{\mathbf{w}} = 1$). A plane wave having "mixed response" (i.e., $\hat{\mathbf{u}} \neq \hat{\mathbf{w}}$) leads to the trivial solution $U = W = 0$ and thus does not exist. We may therefore take $\hat{\mathbf{u}} = \hat{\mathbf{w}}$ for plane waves in a homogeneous material.

9.2.2.1 *Transverse Waves*

Upon placing $\hat{\mathbf{k}}\cdot\hat{\mathbf{u}} = \hat{\mathbf{k}}\cdot\hat{\mathbf{w}} = 0$ in Equation (9.13) we obtain

$$\begin{bmatrix} \rho - Gs^2 & \rho_f \\ \rho_f & \tilde{\rho} \end{bmatrix} \begin{bmatrix} U \\ W \end{bmatrix} = 0, \tag{9.14}$$

which has nontrivial solutions only when the determinant vanishes. This occurs at the complex wave slowness s_s given by

$$s_s^2 = \frac{\rho - \rho_f^2/\tilde{\rho}}{G}. \tag{9.15}$$

When G can be considered real (no mesoscopic or microscopic flow), the imaginary part of s_s is due entirely to relative fluid-solid motion induced by the acceleration of the framework of grains.

The amplitude W of this relative displacement (as normalized by the amplitude U of the displacement of the solid grains) can then be read from Equation (9.14)

$$\frac{W}{U} = i\omega \frac{\rho_f k(\omega)}{\eta} \tag{9.16}$$

where the definition of $\tilde{\rho}$ was used. If it were possible to measure the relative displacement $\mathbf{w}$ of a passing shear wave in addition to the average grain velocity $-i\omega\mathbf{u}$ recorded by a geophone, Equation (9.16) would provide a direct measure of permeability. Unfortunately, a device for measuring $\mathbf{w}$ does not presently exist.

9.2.2.2 *Longtitudinal Waves*
Upon placing $\hat{\mathbf{k}} \cdot \hat{\mathbf{u}} = \hat{\mathbf{k}} \cdot \hat{\mathbf{w}} = 1$ in Equation (9.13) we obtain

$$\begin{bmatrix} Hs^2 - \rho & Cs^2 - \rho_f \\ Cs^2 - \rho_f & Ms^2 - \tilde{\rho} \end{bmatrix} \begin{bmatrix} U \\ W \end{bmatrix} = 0 \tag{9.17}$$

where we have introduced the "undrained" P-wave modulus H as

$$H = K_U + 4G/3. \tag{9.18}$$

An undrained elastic response is one in which fluid exchanges between each sample of the earth and its surroundings do not take place. Again, nontrivial solutions of Equation (9.17) are obtained when the determinant vanishes and this occurs at two values of the slowness that are called here s_{pf} and s_{ps}. Upon solving the quadratic characteristic equations for s^2, one finds that

$$2s^2_{pf,ps} = \gamma \mp \sqrt{\gamma^2 - \frac{4(\tilde{\rho}\rho - \rho_f^2)}{MH - C^2}} \tag{9.19}$$

where taking the "$-$" gives the so-called "fast" P-wave slowness and taking the "$+$" gives the "slow" P-wave slowness and where γ is the auxiliary parameter

$$\gamma = \frac{\rho M + \tilde{\rho} H - 2\rho_f C}{HM - C^2}. \tag{9.20}$$

Equation (9.19) is what allows P-wave attenuation and dispersion to be determined once models for the complex frequency dependence of H, C, and M are determined. When these three moduli are taken to be real and frequency independent, the associated fast-wave attenuation is called "Biot loss" and results entirely from the fluid flow occuring between the peaks and troughs of the wave.

The relative-displacement amplitude W is then read from Equation (9.17)

$$\frac{W}{U} = \beta_{pf,ps} = -\frac{Hs^2_{pf,ps} - \rho}{Cs^2_{pf,ps} - \rho_f}. \tag{9.21}$$

The nature of $\beta_{pf,ps}$ for fast and slow waves is key to understanding the entirely different nature of these two disturbances. It is informative to investigate the $\beta_{pf,ps}$ in the low-frequency limit defined by the dimensionless condition $\omega\rho_f k_o/\eta \ll 1$.

For water in the pores ($\rho_f = 10^3$ kg/m^3 and $\eta = 10^{-3}$ Pa s) and for permeabilities on the order of 10 Darcy or smaller, this limit holds for frequencies satisfying $f < 10^4$ Hz which corresponds to the entire band of interest in exploration seismology. From Equations (9.19)–(9.21), it is straightforward to obtain

$$\beta_{pf} = -\frac{i\omega\rho_f k_o}{\eta}\left(1 + \frac{\rho}{\rho_f}\frac{C}{H}\right)[1 + O(\omega\rho_f k_o/\eta)] \tag{9.22}$$

$$\beta_{ps} = -\frac{H}{C}[1 + O(\omega\rho_f k_o/\eta)]. \tag{9.23}$$

Equation (9.22) shows that in exploration work, the macroscopic relative fluid-solid displacement vanishes for the fast wave, and the response becomes effectively undrained. For the slow wave, the relative fluid-solid displacement is much larger than the displacement of the solid grains (because normally $H \gg C$) and is exactly out of phase with the solid displacement. We will now show that the slow wave at low frequencies is a pure fluid-pressure diffusion and thus not a wave at all.

9.2.2.3 *Understanding the Fast and Slow Response*

As just seen, in either a fast or a slow disturbance the fluid accumulations are related to the volume changes of a sample by the relation

$$\nabla \cdot \mathbf{w} = \beta_{pf,ps} \nabla \cdot \mathbf{u}. \tag{9.24}$$

This relation is also trivially satisfied by the equivoluminal shear waves. If $\nabla \cdot \mathbf{w} = \beta_{pf} \nabla \cdot \mathbf{u}$ is introduced into the governing equations along with Equation (9.22) for β_{pf}, then to leading order in $\omega\rho_f k_o/\eta$, Biot's equations reduce to

$$(K_U + G/3)\nabla\nabla \cdot \mathbf{u} + G\nabla^2\mathbf{u} + \omega^2\rho\mathbf{u} = 0. \tag{9.25}$$

This is exactly the usual elastodynamic wave equation having compressional and shear wave slowness given by the standard expressions

$$s_{pf} = \sqrt{\frac{\rho}{K_U + 4G/3}} \quad \text{and} \quad s_s = \sqrt{\frac{\rho}{G}}. \tag{9.26}$$

If K_U and G are complex and frequency dependent in the seismic band of frequencies due to mesoscopic-scale flow, both of these fast and shear waves will be attenuative despite the response being undrained. Again, the term undrained means only that fluid does not enter or leave an averaging volume and is independent of any fluid redistributions that occur within the averaging volume.

If we introduce $\nabla \cdot \mathbf{w} = \beta_{ps} \nabla \cdot \mathbf{u}$ into the governing equations and use Equation (9.23) for β_{ps}, then to leading order in $\omega\rho_f k_o/\eta$, Biot's equations reduce to

$$\frac{k_o}{\eta} M \left(1 - \frac{C^2}{MH}\right) \nabla^2 p_f + i\omega p_f = 0 \tag{9.27}$$

which is exactly a diffusion equation for the fluid pressure having a fluid-pressure diffusivity given by

$$D = \frac{k_o}{\eta} M \left(1 - \frac{C^2}{MH}\right). \tag{9.28}$$

So in the seismic band of frequencies ($f < 10$ kHz), the slow wave is in fact a pure fluid-pressure diffusion. Because $C^2 \ll MH$, the small correction in the parentheses that is due to fluid-pressure-induced frame expansion is often neglected in hydrology. The undrained P-wave modulus $H = K_U + 4G/3$ depends on the shear modulus. The shear modulus is present in D because fluid-pressure diffusion, like P-wave propagation, is a uniaxial response (a sum of both compression and shear) with no displacements occuring perpendicular to the diffusion front; i.e., all displacement of the solid is in the direction of diffusion. When seismologists or rock physicists talk about a "slow wave," all that is being referred to is hydrological fluid-pressure diffusion.

So the two low-frequency longtitudinal modes of Biot theory correspond to seismology (fast-wave or "P-wave" response) and hydrology (slow-wave response). In the presense of heterogeneity in the porous continuum, seismology and hydrology are coupled (fast waves generate slow waves), and a possible connection between seismic attenuation and permeability can be envisioned. Details of such a possible relation are explored in Section 9.5.

9.3 Relaxation processes in standard Biot theory

The term "standard Biot theory" simply means that the poroelastic moduli K_U, C, M, and G are all real frequency-independent constants as in Biot's (1956a,b, 1962) work. There are two P-wave relaxation processes in this case. One relaxation occurs at the frequency where viscous boundary layers first develop in the pores of a rock and is allowed for within the so-called dynamic permeability $k(\omega)$. The other relaxation occurs when the fluid pressure between the peaks and troughs of a compressional wave just has time to equilibrate during a wave period.

9.3.1 DYNAMIC PERMEABILITY

At low-enough wave frequencies, the relative fluid flow in the pores has a locally "parabolic" flow profile, and the resistance η/k_o to the average fluid-solid movement is entirely a result of the viscous shearing associated with this flow. However, as frequency increases, so does the importance of inertial forces in the local force balance on the fluid (the Navier-Stokes equations that hold throughout the pore space). Since every fluid in earth materials (water, air, natural gas, oil, LNAPL, DNAPL, CO_2) remains attached to the grain surfaces, there develop viscous boundary layers in the pores that connect the purely inertial "plug-profile" flow in the center of the pores to the no-slip condition on the grains surfaces.

Johnson et al. (1987) exactly determine the nature of the flow in the high-frequency limit where viscous-boundary layers become so thin as to be considered locally planar relative to the curved grain surfaces. They connect this exact high-frequency limit to the low-frequency limit (where η/k_o controls the flow resistance) using a simple frequency function that respects causality constraints. Their final model is

$$\frac{k(\omega)}{k_o} = \left[\sqrt{1 - i\frac{4}{n_J}\frac{\omega}{\omega_J}} - i\frac{\omega}{\omega_J}\right]^{-1} \tag{9.29}$$

where the relaxation frequency ω_J, which controls the frequency at which viscous-

boundary layers first develop, is given by

$$\omega_J = \frac{\eta}{\rho_f F k_o}. \tag{9.30}$$

Here, F is exactly the electrical formation factor when grain-surface electrical conduction is not important and is conveniently (though crudely) modeled using Archie's (1942) law $F = \phi^{-m}$. The cementation exponent m is related to the distribution of grain shapes (or pore topology) in the sample and is generally close to 3/2 in clean sands, close to 2 in shaly sands, and close to 1 in rocks having fractured porosity. For an extremely clean sandstone, one might have $\phi = 0.3$ and $k_o = 10^{-12}$ m^2 (1 Darcy) in which case the relaxation frequency is (assuming water in the pores) $f_J = \omega_J/(2\pi) = 10$ kHz which can almost be considered a lower limit for sedimentary rock in the earth. A more common shaly sandstone might have $\phi = 0.15$ and $k_o = 10^{-14}$ m^2 (10 mD) in which case $f_J = 1$ MHz, a value much more typical of consolidated sandstones. Generally, the onset of viscous boundary layers occurs at a frequency well above the seismic band of exploration frequencies (10 Hz to a few kHz) and, as such, it is safe to simply take $k(\omega) = k_o$ for most seismic applications. Note as well that the condition for the neglect of viscous boundary layers $\omega \ll \omega_J$, is equivalent to the low-frequency limit of the Biot theory where the fast-wave becomes an undrained seismic response and the slow-wave becomes a pure fluid-pressure diffusion.

Proper modeling of the remaining parameter n_J in Equation (9.29) is, therefore, not essential in seismic exploration. Nonetheless, this parameter is defined

$$n_J = \frac{\Lambda^2}{k_o F} \tag{9.31}$$

where Λ is a weighted pore-volume to pore-surface ratio with the weight favoring constricted regions of the pore space (the pore throats). See Johnson et al. (1987) for the precise mathematical definition of Λ. The modeling choice of convenience is simply to take $n_J = 8$ for all materials, which is experimentally observed to do a fine job in unconsolidated materials and clean sandstones and is the theoretically expected result for cylindrical tube models of the pore space. In shaly sands, the local pore-volume to pore-surface ratio in the throats becomes smaller, owing to the presence of clays on the grains, and in this case the value of n_J becomes smaller than 8 (potentially much smaller). However, since the precise value of n_J is not of great importance in the seismic band of frequencies, we will not propose here how Λ and k_o might depend on clay content.

The frequency dependence of the attenuation in Biot theory is strongly affected by the nature of $k(\omega)$. Recall that Q^{-1} represents the energy lost to heat in a wave period (Darcy flux multiplied by the fluid-pressure gradient and divided by frequency) as normalized by the strain energy (stress multiplied by strain). In symbols, this may be approximated as

$$Q^{-1} \approx \frac{\mathrm{Re}\{k(\omega)\}}{\omega\eta} \frac{|\nabla p_f \cdot \nabla p_f|}{H|\nabla \cdot \mathbf{u}|^2} \tag{9.32}$$

$$\approx \frac{\omega\rho \mathrm{Re}\{\mathrm{k}(\omega)\}}{\eta} \left(\frac{C}{H}\right)^2 \tag{9.33}$$

where a P wavelength of $\lambda = 2\pi\sqrt{(H/\rho)}/\omega$ was used in estimating the pressure gradient, and it is assumed that fluid-pressure equilibration at the scale of the wavelength does not have time to occur at each frequency.

Now the exact high-frequency asymptotic behavior of $k(\omega)$ has real and imaginary parts given by

$$k(\omega) \sim \sqrt{\frac{2}{n_J}} \left(\frac{\omega_J}{\omega}\right)^{3/2} + i\frac{\omega_J}{\omega} \qquad \text{as} \quad \frac{\omega_J}{\omega} \to 0. \tag{9.34}$$

Equation (9.33) then shows that when $\omega \ll \omega_J$, Q^{-1} increases linearly with frequency because $\mathrm{Re}\{k(\omega)\} \to k_o$. However, when $\omega \gg \omega_J$, Q^{-1} decreases as the square root of frequency because $\mathrm{Re}\{k(\omega)\}$ decreases as $\omega^{-3/2}$. This behavior is also seen in the exact results based on Equation (9.19) displayed in Figure 9.1 for the curve $\omega_B/\omega_J > 1$.

9.3.2 WAVELENGTH-SCALE FLUID-PRESSURE EQUILIBRATION

The other relaxation in standard Biot theory occurs when (and if) the fluid pressure between the peaks and troughs of the wave just has time to equilibrate in a wave period.

To approximate the frequency $\omega_B = 2\pi f_B$ at which this occurs, we can use the standard result of any diffusion process $\tau = L^2/D$ for the time τ required to diffuse a distance L into a material having a diffusivity D. In the case of a P wave, the distance to be equilibrated L is roughly half of one wavelength λ, which is stated (for algebraic convenience) as $L \approx \lambda/\sqrt{2\pi}$. Now, $\lambda \approx \sqrt{H/\rho}/f$, where f is the wave frequency (Hertz) and the diffusivity is roughly $D \approx Mk_o/\eta$. Thus, the critical frequency is defined when $1/f_B = \tau = \lambda^2/(2\pi D) = H/(2\pi D\rho f_B^2)$ or

$$\omega_B = \frac{H}{M}\frac{\eta}{\rho k_o}. \tag{9.35}$$

Comparing the expressions for ω_J and ω_B, one obtains

$$\frac{\omega_B}{\omega_J} = \frac{H}{M}\frac{\rho_f}{\rho}F. \tag{9.36}$$

When $\omega_B < \omega_J$, the wavelength-scale equilibration occurs at a lower frequency than the onset of viscous boundary layers. In this case, as the wave frequency becomes greater than ω_B, the fluid-pressure equilibrates rapidly in each wave period and the seismic response becomes increasingly drained (i.e., as if the fluid in the pores were no longer present). Accordingly, the velocity decreases when $\omega > \omega_B$ as is seen in Figure 9.1 for the curve $\omega_B/\omega_J = 0.1$. When $\omega_B > \omega_J$, the viscous boundary layers develop and the attenuation peaks and begins to fall as the square root of frequency before wavelength-scale equilibration ever has a chance to occur. In this case, the wavelength-scale equilibration never has time to occur at any frequency. Such behavior is also demonstrated in Figure 9.1 using Equation (9.19) for the complex slowness. For most sedimentary rocks, ω_B/ω_J as given by Equation (9.36) is close to, but greater than, unity.

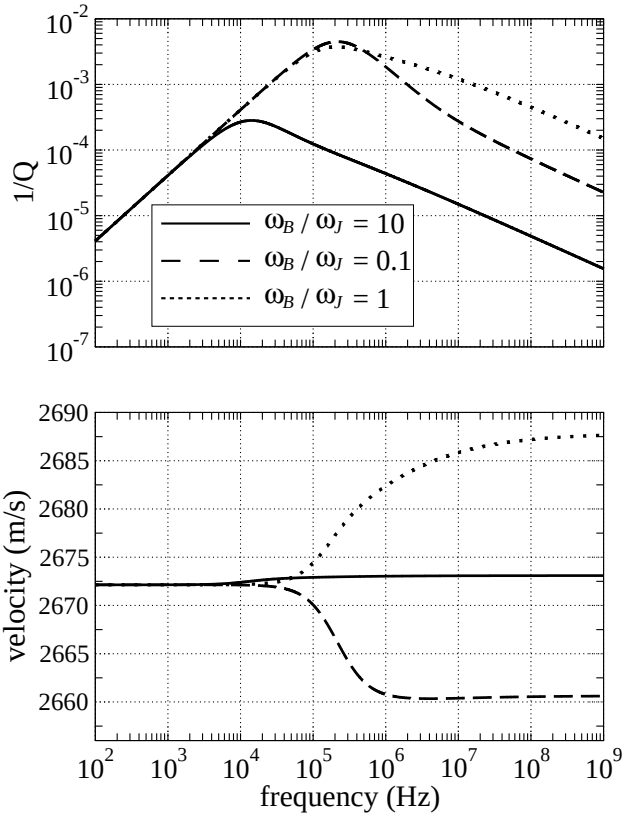

Figure 9.1: Various types of dispersion curves in standard Biot theory. The most common situation in porous rocks is that $\omega_B/\omega_J > 1$ (i.e., viscous boundary layers develop in the pores at a lower frequency compared to when fluid-pressure equilibration at the scale of the wavelength has time to occur). The material properties here correspond to a weakly consolidated sandstone; however, to achieve the unusual condition that $\omega_B/\omega_J = 0.1$, we took the shear modulus to be several times smaller than and the fluid-pressure diffusion modulus M to be several times larger than in the other two curves.

However, the level of dispersion and attenuation associated with these effects is almost totally negligible in the seismic frequency band of interest. Attenuation-dispersion mechanisms of more pertinence to seismic exploration are the focus of Section 9.5.

9.4 The quasi-static poroelastic moduli

In naturally occuring rocks, the three poroelastic incompressibilities K_U, C, and M, as well as the shear modulus G of the material, will be complex and frequency dependent due to both mesoscopic and squirt flow. Only in the special case of porous materials having uniform frame properties and being free of grain-

scale cracks/damage (such as in some artificially created "rocks") will these elastic moduli be real constants at all frequencies. Alternatively, for real rocks in the limit of very low frequencies (possibly below the seismic band of frequencies), the imaginary parts of these moduli will tend to zero and the real parts will become frequency-independent constants. The present section concerns this low-frequency (quasi-static) limit, where fluid pressure may be taken as uniform throughout a porous rock sample.

9.4.1 THE THREE POROELASTIC INCOMPRESSIBILITIES

A multitude of names have been given to the three incompressibilities of poroelasticity (here denoted as K_U, C, and M), which sometimes makes the theory seem more difficult than it really is. From both a laboratory and pedagogic perspective, the three moduli that have the clearest definition are

$$K_U = -\left(\frac{\delta P_c}{\delta V/V_o}\right)_{\nabla\cdot\mathbf{w}=0} \tag{9.37}$$

$$K_D = -\left(\frac{\delta P_c}{\delta V/V_o}\right)_{\delta p_f=0} \tag{9.38}$$

$$B = \left(\frac{\delta p_f}{\delta P_c}\right)_{\nabla\cdot\mathbf{w}=0}. \tag{9.39}$$

The modulus K_U is called the "undrained bulk modulus" because it is defined under the condition $\nabla \cdot \mathbf{w} = 0$ where fluid is not allowed to either enter or leave the sample during deformation. Recall that $\nabla \cdot \mathbf{u} = \delta V/V_o$ where δV is the volume change of a sample that initially occupied a volume V_o. The modulus K_D is called the "drained bulk modulus" and is defined under the condition that the fluid pressure in a sample does not change. The modulus K_D is thus not affected by the presence of fluid in the rock. A drained experiment with any of oil, water or air in the pores should all produce the same value for K_D. Last, the undrained fluid-pressure to confining-pressure ratio B is called "Skempton's coefficient," after the work of Skempton (1954).

These three moduli can be conveniently measured in the lab (c.f., Wang, 2000). An impermeable jacket is usually fitted around a lab sample and a tube is inserted through the jacket allowing the fluid in the pores to be connected to a reservoir whose pressure p_f may be controlled and measured. The jacketed sample is then immersed in a second fluid reservoir characterized by a confining pressure P_c. First, an increment δP_c is applied in such a manner that no fluid flows through the tube (this is done by controlling the pressure p_f). The change in volume of the jacketed sample is recorded to give K_U and the fluid pressure increment δp_f is read off to give B. Next, δp_f is returned to zero, allowing fluid to flow through the tube. The subsequent change in sample volume then yields K_D.

Using these definitions, it is easy to demonstrate that the moduli C and M in Equations (9.4)–(9.5) are given by

$$C = BK_U \quad \text{and} \quad M = BK_U/\alpha \tag{9.40}$$

where the new constant α is called the "Biot-Willis constant," after Biot and Willis (1957), and is exactly defined as

$$\alpha = \left(\frac{\delta P_c}{\delta p_f}\right)_{\nabla \cdot \mathbf{u}} = \frac{1 - K_D/K_U}{B}. \tag{9.41}$$

Berge et al. (1993) have demonstrated the not-so-obvious and important fact that although K_U and B are both dependent on the type of fluid in the pores, α is not. All of these definitions and relations are independent of the possible presence of anisotropy at either the sample or grain scale, and are also independent of whether the grains making up the rock have different mineralogies. The modulus M is called the "fluid-storage coefficient," since it represents how much fluid can accumulate in a sample when the fluid-pressure changes at constant sample size. It is the elastic modulus principally involved in fluid-pressure diffusion, as Equation (9.27) demonstrates. There is no standard name for the modulus C other than Biot's (1962) "coupling modulus."

It is sometimes convenient to rewrite the incompressibility laws [Equations (9.4) and (9.5)] as compressibility laws

$$\begin{pmatrix} \nabla \cdot \mathbf{u} \\ \nabla \cdot \mathbf{w} \end{pmatrix} = \frac{1}{K_D} \begin{pmatrix} 1 & -\alpha \\ -\alpha & \alpha/B \end{pmatrix} \begin{pmatrix} -\delta P_c \\ -\delta p_f \end{pmatrix}. \tag{9.42}$$

We often use K_D, B, and α as the fundamental suite of three poroelastic constants.

9.4.2 THE BIOT-GASSMANN FLUID SUBSTITUTION RELATIONS

From the perspective of connecting seismic velocities and hydrological properties, the pioneering contribution of Gassmann (1951) is without rival. Gassmann showed that if the solid material making up the grains is both isotropic and uniform throughout a sample, then in the limit of low-frequencies the undrained modulus K_U and Skempton's coefficient B are frequency-independent constants that can be exactly expressed in terms of the drained modulus K_D, the porosity ϕ, the mineral modulus of the grains K_s, and the fluid modulus K_f

$$B = \frac{1/K_D - 1/K_s}{1/K_D - 1/K_s + \phi(1/K_f - 1/K_s)}, \tag{9.43}$$

$$K_U = \frac{K_D}{1 - B(1 - K_D/K_s)}. \tag{9.44}$$

From these results, one also has $\alpha = 1 - K_D/K_s$ which is indeed seen to be independent of K_f. The importance of Equations (9.43) and (9.44) is that all dependence on the fluid type is entirely confined to the fluid modulus K_f. These relations tell us how the poroelastic incompressibilities change when one fluid is substituted for another. Gassmann also made the reasonable assumption that at sufficiently low frequencies, the fluid has no influence on the shear modulus G.

After some algebra, the following forms for the Biot-Gassmann incompressibil-

ities are instructive

$$K_U = \frac{K_D + [1-(1+\phi)K_D/K_s]\,K_f/\phi}{1+\Delta}, \tag{9.45}$$

$$C = \frac{(1-K_D/K_s)K_f/\phi}{1+\Delta}, \tag{9.46}$$

$$M = \frac{K_f/\phi}{1+\Delta}, \tag{9.47}$$

where Δ is a dimensionless parameter defined as

$$\Delta = \frac{1-\phi}{\phi}\frac{K_f}{K_s}\left(1-\frac{K_D}{(1-\phi)K_s}\right). \tag{9.48}$$

These are called the "Biot-Gassmann" relations, because although Gassmann (1951) treated K_U and C, it was Biot and Willis (1957) who first treated M (Gassmann only considered the undrained response). These particular algebraic forms are useful because Δ is always a small number. In an extreme stiff-frame limit defined by $K_D \to (1-\phi)K_s$ (which actually lies above the Hashin and Shtrikman, 1963, upper bound), $\Delta \to 0$. The opposite limit of an infinitely compliant frame $K_D \to 0$ occurs when the grains no longer form connected paths across the sample. In sediments, this percolation threshhold occurs when $\phi \approx 0.5$ with the precise value depending on details of the grain-size distribution and packing configuration. Thus, Δ takes its largest value of K_f/K_s when there is an infinitely compliant frame and is never outside the range $0 < \Delta < K_f/K_s$ for any material type. For a liquid, one generally has $K_f/K_s \approx 10^{-1}$ while for a gas, $K_f/K_s \approx 10^{-5}$.

Equations (9.45)–(9.47) demonstrate that $K_U \geq M \geq C$ in a Gassmann material. Only for very soft unconsolidated materials in which $K_D \ll K_f/\phi$, does one obtain $K_U \approx M \approx C$.

9.4.3 THE DRAINED BULK MODULUS K_D AND SHEAR MODULUS G

For the fluid-substitution relations to be useful in interpreting and/or inverting seismic data, it will usually be necessary to have a theoretical model for K_D. In the low-frequency limit, both K_D and G depend only on the microgeometry of how the framework of grains is put together and on the minerals making up the grains. There exists a vast literature surrounding the various theoretical models for such "frame moduli" (c.f., Berryman, 1995, and Mavko et al., 1998). No one universal model is valid for all porous materials. The goal here is restricted to recommending a few simple models that are consistent with data.

The single most important factor in choosing a theoretical model for K_D and G is whether or not the grains are cemented together; i.e., is the material consolidated or unconsolidated?

9.4.3.1 *Unconsolidated Materials*

If a material is unconsolidated (e.g., a sandpack or soil), the stress concentration and deformation in the micron-scale regions surrounding the individual grain-to-grain contact points is what controls the overall deformation. Such contact points

are most often modeled as idealized sphere-to-sphere "Hertzian" contacts from which theoretical results for the overall packing can be approximately derived. A key concept is that the area of the individual grain contacts increases with effective stress $P_e = P_c - p_f$ (see Section 9.4.5 for a discussion of effective stress). As the grain-contact area increases, both the contact and the material become stiffer and more rigid. Data on natural sands (e.g., Hardin and Richart, 1963; Domenico, 1977) indicate that both G and K_D increase with effective stress as $P_e^{1/2}$ for $0 < P_e < P_o$, where P_o is observed to be on the order of 10 MPa (corresponding to a depth of roughly 1 km). For $P_e > P_o$, both G and K_D roll over to a more gradual $P_e^{1/3}$ increase.

For natural soils having a spectrum of grain sizes, there need not be a clear relation between the porosity and the frame moduli. Imagine a packing of large 500 μm sand grains. If smaller 10 μm grains are loosely present in the voids between the larger grains, but do not act as stress bridges, they can markedly change the porosity of the soil while leaving the frame moduli effectively unchanged. Most theoretical models are based on packings of single-radius spheres, in which case known relations exist between the porosity and the type of packing.

Walton (1987) has produced perhaps the simplest model for a random packing of identical spheres

$$K_D = \frac{1}{6}\left[\frac{3(1-\phi_o)^2 n^2 P_e}{\pi^4 C_s^2}\right]^{1/3} \quad \text{and} \quad G = RK_D \tag{9.49}$$

where n is the average number of contacts per grain known as the "coordination number," ϕ_o is the porosity of the random packing at $P_e = 0$, and C_s is a compliance parameter defined as

$$C_s = \frac{1}{4\pi}\left(\frac{1}{G_s} + \frac{1}{K_s + G_s/3}\right) \tag{9.50}$$

where G_s and K_s are the single-mineral moduli of the grains. The parameter R takes on a value somewhere in the range

$$\frac{3}{5} \leq R \leq \frac{18}{5}\left(\frac{K_s + G_s}{3K_s + 2G_s}\right) \tag{9.51}$$

where the lower limit corresponds to grains so smooth that tangential slip always occurs which prevents shear force from being transmitted at the contact, and the upper limit corresponds to grains so rough that no slip occurs which results in a maximum transmitted shear at a contact. Our experience is that the lower limit of $R = 3/5$ does a somewhat better job matching data.

Walton (1987) derived these results assuming that n was a constant (all contacts in place at $P_e = 0$). His result is at odds with the experimentally observed $P_e^{1/2}$ dependence when $P_e < P_o$ which corresponds to the entire depth range of interest in hydrogeophysics. One way to account for the observed pressure dependence is to assume that the average coordination number increases with the negative dilatation $\epsilon = -\nabla \cdot \mathbf{u}$ of the material. At $P_e = 0$, the material is assumed to have, effectively, no contacts in place, but as the material is compressed,

the contacts between the grains are created. Goddard (1990) has proposed that stress-free grain rotations create grain-to-grain contacts that result in the law

$$n(\epsilon) = \begin{cases} n_o \left(\epsilon/\epsilon_o\right)^{1/2} & \text{when } P_e \ll P_o, \\ n_o & \text{when } P_e \gg P_o, \end{cases} \tag{9.52}$$

where ϵ_o is the negative dilatation when $P_e = P_o$ and where n_o is the maximum number of contacts per grain that can arrive. Using this law within the Walton (1987) theory gives the relation between dilatation and pressure to be $\epsilon(P_e) = \{6\pi^2 C_s \epsilon_o^{1/2} P_e/[(1-\phi_o)n_o]\}^{1/2}$ whenever $P_e \ll P_o$. It is then straightforward to re-express the Walton result as

$$K_D = \frac{1}{6}\left[\frac{4(1-\phi_o)^2 n_o^2 P_o}{\pi^4 C_s^2}\right]^{1/3} \frac{(P_e/P_o)^{1/2}}{\{1+[16P_e/(9P_o)]^4\}^{1/24}} \tag{9.53}$$

which is a new result, though anticipated by Goddard (1990). The new parameter compared to Walton's (1987) theory is P_o, which is the pressure beyond which $n = n_o$ and no new contacts are created. It is taken here as an empirical constant on the order of 10 MPa in sands. If we put $P_o = 0$, the Walton result [Equation (9.49)] is exactly recovered. The exponents of 4 and 1/24 in the denominator of Equation (9.53) were chosen somewhat arbitrarily, the only requirement being that their product is 1/6. (If we use 8 and 1/48, for example, the results are imperceptibly different.)

Equation (9.53), along with $G = 3K_D/5$, is our recommendation for the drained moduli of unconsolidated materials which are the key properties affecting wave speeds in hydrogeophysics. If the same values for K_s and G_s are always employed (a reasonable modeling choice), there are two free parameters; namely, P_o and $(1-\phi_o)n_o$. For random sand packs, we have $0.32 < \phi_o < 0.38$ and $8 < n_o < 11$.

In Figure 9.2, this model with $P_o = 18$ MPa, $R = 3/5$, $\phi_o = 0.36$, $n_o = 9$, $K_s = 37$ GPa, and $G_s = 44$ GPa is compared to data collected by Murphy (1982) on a random glass-bead pack in which the bead-diameters ranged from 74 to 105 μm (common soil grain sizes) and in which the pore space was empty. Murphy (1982) chose this pressure range because it exhibits the $P_e^{1/2}$ to $P_e^{1/3}$ transition in the modulus dependence. The theory does an adequate job of modeling this transition. Particularly interesting is that the model parameters have not been adjusted to give an optimal fit; they are the parameters one *a priori* expects to hold for a dense random pack of identical quartz spheres. Although, the difference between Equation (9.53) and Equation (9.49) appears to be minimal in this example, if the velocities are determined over the lower-pressure ranges of interest in hydrogeophysics, there is a pure $P_e^{1/2}$ modulus dependence, as has been documented in many data sets including Hardin and Richart (1963) and Domenico (1977).

In conclusion, we emphasize that Equation (9.53) is entirely independent of grain size and, therefore, permeability (permeability depends on the size of the pores and, therefore, grains). Thus, the predicted low-frequency seismic velocities for any unconsolidated material having a unimodal grain-size distribution is

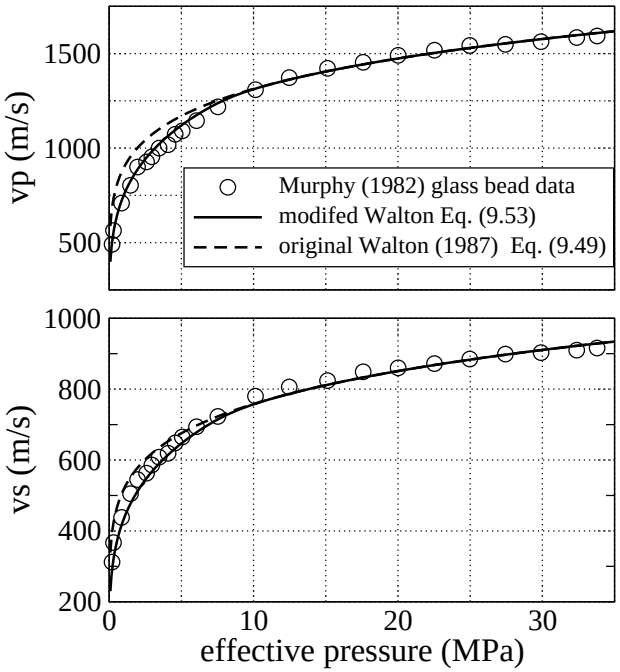

Figure 9.2: Comparison of the Murphy (1982) data set on a dry glass-bead pack to the theoretical model discussed in the text. The $P_e^{1/2} \rightarrow P_e^{1/3}$ transition occurs at an effective pressure of 10 MPa corresponding to P_o = (16/9)10 MPa $\approx$ 18 MPa.

expected to be independent of grain size and permeability, as has been experimentally demonstrated by Murphy (1982) using glass-bead packs.

But, as is shown in Chapter 13 of this volume, field measurements of permeability and seismic velocities indicate the two are sometimes at least weakly correlated in unconsolidated sediments (although in some cases the observed correlation is positive, while in others it is negative). Presently existing models for the seismic velocities in unconsolidated sediments are all based on single grain-size distributions. Any link between permeability and velocity must necessarily come from having a spectrum of grain sizes present. Unfortunately, statistical relations between grain-size distribution and quantities like average number of contacts per grain are generally not available since they depend strongly on how the grain packing was prepared. Possible connections between permeability and seismic wave speeds will be more thoroughly discussed in Section 9.6.

9.4.3.2 *Consolidated Materials*

In a consolidated material, diagenetic clay or quartz has been deposited around the grain contacts, and the Hertzian nature of such contacts is largely if not entirely removed. The material in this case behaves more like a pure solid with cavities. Numerous effective-medium theories (e.g., Berryman, 1980a,b) have been proposed that treat how various shaped cavities (mostly ellipsoidal) at various volume frac-

tions influence the drained moduli. Although such embedded cavities do not form a connected porosity as in real rocks, they are often used in estimating the drained frame moduli so long as each cavity is empty. Upon using sufficient numbers of relatively stiff spherical cavities and relatively compliant penny-shaped cavities, effective-medium models can usually predict fairly well the measured frame moduli of consolidated rock including the pressure dependence (which is controlled largely by crack closure).

Models based on randomly placed ellipsoidal inclusions often have the implicit form $K_D = f_1(K_D, G, K_s, G_s, a_r, \phi)$ and $G = f_2(K_D, G, K_s, G_s, a_r, \phi)$ where a_r is the aspect ratio of the embedded cavities and ϕ the porosity. The functions f_1 and f_2 are different depending on the theory, but are highly nonlinear in the variables. Uncoupled analytical expressions for K_D and G are generally not available. If a spectrum of ellipsoidal shapes are to be included (e.g., Toksoz et al., 1976), the model becomes even more complicated.

Our recommendation is to work with the following simple forms

$$K_D = K_s \frac{1-\phi}{1+c\phi} \quad \text{and} \quad G = G_s \frac{1-\phi}{1+3c\phi/2} \tag{9.54}$$

where the parameter c is called the "consolidation parameter," since it characterizes the degree of consolidation between the grains. Again, it seems a reasonable modeling choice to fix K_s and G_s and to only allow the consolidation parameter c and porosity ϕ to change from one rock type to the next (though one may want to distinguish between carbonates for which $K_s \approx 2G_s$ and silicate grains for which $K_s \approx G_s$). Effective-medium theories (e.g., Korringa et al., 1979; Berryman, 1980a,b) can be approximately manipulated into expressions of this form and predict that c depends both on the shape of the cavities and the ratio G_s/K_s. The factor of $3/2$ in the expression for G is somewhat arbitrary (working with $5/3$ or 2 is also reasonable) but yields plots of P-wave velocity versus S-wave velocity that are consistent with data on sandstones (e.g., Castagna et al., 1993). Depending on the degree of cementation, one can expect the approximate range $2 < c < 20$ for consolidated sandstones (2 being extremely consolidated and 20 poorly consolidated). An unconsolidated sand in this model can require $c \gg 20$ in which case it may be more appropriate to use the above modified Walton theory [Equation (9.53)]. The frame moduli for various ϕ and c in this model are given in Figure 9.3. With K_s and G_s fixed, both ϕ and c become the targets of seismic inversion.

9.4.4 POROSITY CHANGE

A general expression exists for how porosity changes $\delta\phi$ are related to changes in confining pressure δP_c and fluid pressure δp_f. This is a central result of poroelasticity that is useful in hydrological (and other) applications of poroelasticity, even if it is not directly needed in modeling linear wave propagation.

Let V_ϕ define the pore volume within a sample of total volume V. By definition, the porosity is $\phi = V_\phi/V$. Taking the derivative yields $\delta\phi = \delta V_\phi/V - \phi\delta V/V$ where $\delta V/V = \nabla \cdot \mathbf{u}$. The only way the pore volume changes is if the increment of fluid

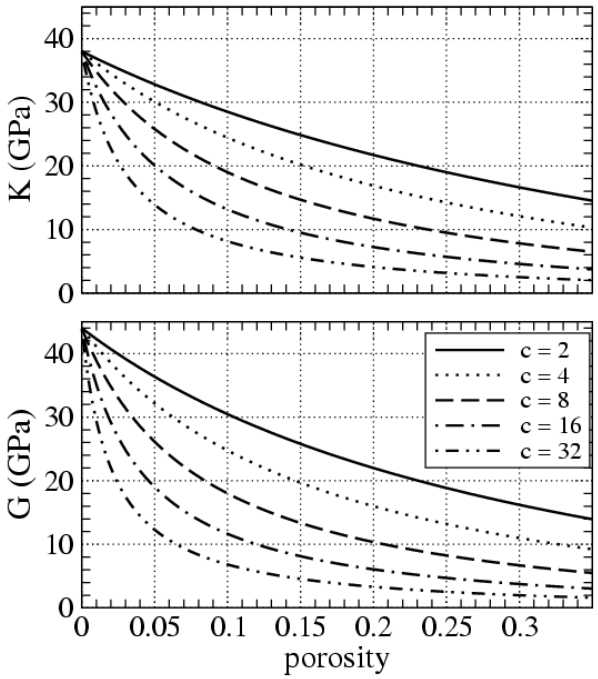

Figure 9.3: The frame moduli of Equation (9.54) for various porosities and consolidation factors c. The solid was taken to be quartz ($K_s = 38$ GPa and $G_s = 44$ GPa).

content $-\nabla \cdot \mathbf{w}$ differs from the fluid volume change due to compression $\phi \delta p_f / K_f$. Thus,

$$\delta\phi = -\phi \nabla \cdot \mathbf{u} - \nabla \cdot \mathbf{w} - \phi \delta p_f / K_f \tag{9.55}$$

which, when combined with the compressibility laws of Equation (9.42), gives exactly

$$\delta\phi = -C_\phi \left(\delta P_c - \alpha_\phi \delta p_f \right) \tag{9.56}$$

where the porosity compliance C_ϕ is defined as

$$C_\phi = \frac{1}{B} \left(\frac{1}{K_D} - \frac{1}{K_U} \right) - \frac{\phi}{K_D} \tag{9.57}$$

and where the porosity effective-stress coefficient α_ϕ is

$$\alpha_\phi = \frac{\phi/K_f + (\phi - 1/B)(1/K_D - 1/K_U)/B}{\phi/K_D - (1/K_D - 1/K_U)/B}. \tag{9.58}$$

In the special case of a Gassmann material [mono-mineral isotropic grains for which Equations (9.43) and (9.44) apply], one then has the convenient result

$$C_\phi = \frac{1-\phi}{K_D} - \frac{1}{K_s} \qquad \text{and} \quad \alpha_\phi = 1. \tag{9.59}$$

Note that the porosity changes being modeled here are the purely elastic reversible changes. The actual porosity variation with depth in the crust is controlled almost exclusively by diagenetic changes (deposition and dissolution of minerals). The usefulness of Equation (9.56) is for modeling porosity change when fluids are being pumped into or out of sand formations, such as in CO_2 sequestration.

9.4.5 EFFECTIVE STRESS

Effective stress refers to what linear combination of confining pressure change δP_c and fluid pressure change δp_f are required to affect change of a particular material property. So far, we have seen three effective-stress laws; namely, the law for how the volume V of a sample changes,

$$-\frac{\delta V}{V} = -\nabla \cdot \mathbf{u} = \frac{1}{K_D}\left(\delta P_c - \alpha \delta p_f\right), \tag{9.60}$$

the law for how much fluid volume δV_ζ either enters or leaves a porous sample,

$$\frac{\delta V_\zeta}{V} = \nabla \cdot \mathbf{w} = \frac{\alpha}{K_D}\left(\delta P_c - \frac{1}{B}\delta p_f\right), \tag{9.61}$$

and the just-mentioned law for how the porosity changes $\delta\phi = -C_\phi\left(\delta P_c - \alpha_\phi \delta p_f\right)$ where C_ϕ and α_ϕ are defined in Equations (9.57) and (9.58).

All porous material properties change to some degree when either δP_c or δp_f change and there is an effective-stress variable $\delta P_c - \alpha_\pi \delta p_f$ for each such property π (c.f., Berryman, 1992). Alternatively stated, if $\delta P_c = \alpha_\pi \delta p_f$, property π will not change. The coefficient α_π is known as the effective-stress coefficient of the property π (note that the effective-stress coefficient for volume change is $\alpha_V = \alpha$ which is what we also call the Biot-Willis constant).

In near-surface hydrological problems, the relatively soft materials are quite sensitive to the fluid-pressure changes, and it is of interest from a monitoring perspective to know how the geophysical properties of the subsurface are changing due to fluid-pressure changes caused, for example, by pumping.

Any physical property that is scale invariant (i.e., a property that does not change if the grain space is uniformly expanded or contracted) should have an effective-stress variable $\delta P_c - \alpha_\phi \delta p_f$ that is identical to the porosity variable since porosity is scale invariant (Berryman, 1992). Such properties include soil density, electrical conductivity, and the low-frequency and high-frequency limits of the poroelastic moduli. Since $\alpha_\phi = 1$ in a Gassmann material (isotropic mono-mineral grains), the effective-stress combination $\delta P_c - \delta p_f$ is often employed (such as in Section 9.4.3.1 for the drained moduli of unconsolidated sands). So the general rule for a scale-invariant property π that, accordingly, depends only on the porosity ϕ is that $\delta\pi = [d\pi(\phi)/d\phi]\,\delta\phi$, where the porosity change $\delta\phi$ is given by Equation (9.56) and where the derivative $d\pi/d\phi$ requires a model for the property $\pi(\phi)$.

Permeability is an important example of a material property that is not scale invariant. The general form of the permeability (e.g., Thompson et al., 1987) is $k = \ell^2/F$, where F is the electrical formation factor and ℓ is some appropriately

defined pore-throat dimension. This gives

$$\frac{\delta k}{k} = 2\frac{\delta \ell}{\ell} - \frac{\delta F}{F}. \tag{9.62}$$

Upon stressing the material, the length ℓ will change only if the pore volume V_ϕ changes. Thus, it is reasonable to assume that $\ell = \text{const}\, V_\phi^{1/3}$ which results in

$$\frac{\delta \ell}{\ell} = \frac{1}{3}\frac{\delta V_\phi}{V_\phi} = -\frac{1}{3}\left(\frac{\nabla \cdot \mathbf{w}}{\phi} + \frac{\delta p_f}{K_f}\right). \tag{9.63}$$

If Archie's (1942) law $F = \phi^{-m}$ for the electrical formation factor is employed, one obtains

$$\frac{\delta F}{F} = -m\frac{\delta \phi}{\phi} = m\left(\frac{\nabla \cdot \mathbf{w}}{\phi} + \frac{\delta p_f}{K_f} + \nabla \cdot \mathbf{u}\right). \tag{9.64}$$

Putting this together then gives an effective-stress model for permeability

$$\frac{\delta k}{k} = -\frac{[2\alpha/3 + m(\alpha - \phi)]}{\phi K_D}\left(\delta P_c - \alpha_k \delta p_f\right) \tag{9.65}$$

where

$$\alpha_k = \frac{\phi\alpha m - (2/3 + m)(\alpha/B - \phi)}{\phi m - (2/3 + m)\alpha} \tag{9.66}$$

is the effective-stress coefficient for permeability in the model.

9.5 Attenuation and dispersion in the seismic band of frequencies

The intrinsic attenuation Q^{-1} so far allowed for in standard Biot theory is inadequate to explain the levels of attenuation observed on seismograms in the field.

For transmission experiments (VSP, crosswell tomography, sonic logs), the total attenuation inferred from the seismograms can be decomposed as $Q^{-1}_{\text{total}} = Q^{-1}_{\text{scat}} + Q^{-1}$ where both the scattering and intrinsic contributions are necessarily positive. In transmission experiments, multiple scattering transfers energy from the coherent first-arrival pulse into the coda and into directions that will not be recorded on the seismogram, and is thus responsible for an effective "scattering attenuation" Q^{-1}_{scat}. Techniques have been developed that attempt to separate the intrinsic loss from the scattering loss in transmission experiments (e.g., Wu and Aki, 1988, and Sato and Fehler, 1998). In seismic reflection experiments, back-scattered energy from the random heterogeneity can sometimes act to enhance the amplitude of the primary reflections. At the present time, techniques that can reliably separate the total loss inferred from reflection experiments into scattering and intrinsic portions are not available.

Inverting seismic data for attenuation is not yet standard practice and there are only a limited number of published examples. Quan and Harris (1997) use tomography to invert the amplitudes of crosswell P-wave first arrivals to obtain the Q^{-1} for the layers of a stratified sequence of shaly sandstones and limestones (depths ranging from 500–900 m). Crosswell experiments in such horizontally stratified sediments produce negligible amounts of scattering loss so that essentially

all apparent loss (except for easily corrected spherical spreading) is attributable to intrinsic attenuation. The center frequency in the Quan and Harris (1997) measurements is roughly 1750 Hz, and they find that $10^{-2} < Q^{-1} < 10^{-1}$ for all the layers in the sequence. Sams et al. (1997) have also measured the intrinsic loss in a stratified sequence of water-saturated sandstones, siltstones and limestones (depths ranging from 50–250 m) using VSP (30–280 Hz), crosswell (200–2300 Hz), sonic logs (8–24 kHz), and ultrasonic laboratory (500–900 kHz) measurements. They calculate that in the VSP experiments, $Q^{-1}/Q_{\rm scat}^{-1} \approx 4$, while in the sonic experiments, $Q^{-1}/Q_{\rm scat}^{-1} \approx 19$; i.e., for their sequence of sediments, the intrinsic loss dominates the scattering loss at all frequencies. Sams et al. (1997) also find that $10^{-2} < Q^{-1} < 10^{-1}$ across the seismic band.

One way to explain these measured levels of intrinsic attenuation in the seismic band is if mesoscopic heterogeneity is present within each averaging volume. A P wave creates a larger fluid-pressure change where the sediments are relatively more compliant than where they are relatively more stiff. A fluid pressure equilibration ensues that attenuates wave energy. This mechanism has a Q^{-1} that can peak anywhere within the seismic band, depending on the length scale of the heterogeneity and the permeability of the material. White et al. (1975), Norris (1993), Gurevich and Lopatnikov (1995) and Gelinsky and Shapiro (1997) have all modeled such mesoscopic loss in the case of waves normally incident to a sequence of thin porous layers.

The approach taken here is to model the mesoscopic-scale heterogeneity as an arbitrary mixture of two porous phases. Each porous phase is assumed to locally obey Biot's Equations (9.1)–(9.5) and both porous phases are present in an averaging volume of the earth. In this case, Pride and Berryman (2003a,b), following up on work by Berryman and Wang (1995), have shown that the macroscopic-scale compressibility laws (the laws controlling the response of each sample of a two-porous phase composite) are

$$\begin{bmatrix} \nabla\cdot\mathbf{v} \\ \nabla\cdot\mathbf{q}_1 \\ \nabla\cdot\mathbf{q}_2 \end{bmatrix} = i\omega \begin{bmatrix} a_{11} & a_{12} & a_{13} \\ a_{12} & a_{22} & a_{23} \\ a_{13} & a_{23} & a_{33} \end{bmatrix} \cdot \begin{bmatrix} P_c \\ \overline{p}_{f1} \\ \overline{p}_{f2} \end{bmatrix} + i\omega \begin{bmatrix} 0 \\ \zeta_{\rm int} \\ -\zeta_{\rm int} \end{bmatrix}, \tag{9.67}$$

$$-i\omega\zeta_{\rm int} = \gamma(\omega)\,(\overline{p}_{f1} - \overline{p}_{f2}). \tag{9.68}$$

Here, $\mathbf{v}$ is the average particle velocity of the solid grains throughout an averaging volume, $\mathbf{q}_i$ is the average Darcy flux across phase i, P_c is the average total pressure acting on the averaging volume, $\overline{p}_{fi}$ is the average fluid pressure within phase i, and $-i\omega\zeta_{\rm int}$ is the average rate at which fluid volume is being transferred from phase 1 into phase 2 as normalized by the total volume of the averaging region. The dimensionless increment $\zeta_{\rm int}$ represents the "mesoscopic flow."

The compressibilities a_{ij} are real and control the elastic response at high frequencies before there is time for fluid-pressure equilibration between the two porous phases to occur. The internal transport coefficient $\gamma(\omega)$ controls the rate at which fluid is being transferred from one porous phase to the other within a porous sample. It is complex and frequency dependent, and has been shown by

Pride and Berryman (2003b) and Pride et al. (2004) to take the form

$$\gamma(\omega) = \gamma_o \sqrt{1 - i\frac{\omega}{\omega_o}}. \tag{9.69}$$

At sufficiently high frequencies defined by $\omega \gg \omega_o$, the fluid-pressure diffusion penetrates only a small distance from one phase into the other during a wave cycle. At sufficiently low frequencies defined by $\omega \ll \omega_o$, the fluid-pressure front has time to advance through the entire sample during a wave cycle and the final stages of equilibration are better characterized as nearly uniform fluid-pressure gradients that are quasi-statically decreasing in amplitude until they ultimately vanish in the dc limit. Models for the a_{ij}, γ_o, and the transition frequency ω_o will be presented in the sections that follow in various geometrical circumstances.

We now reduce these "double-porosity" compressibility laws to an effective Biot theory having complex frequency-dependent coefficients. The easiest way to do this is to assume that phase 2 is entirely embedded in phase 1, so that the flux $\mathbf{q}_2$ into and out of the averaging volume is zero. By placing $\nabla \cdot \mathbf{q}_2 = 0$ into the compressibility laws of Equation (9.67), the fluid pressure $\overline{p}_{f2}$ can be entirely eliminated from the equations. If we then introduce the average solid displacement $\mathbf{u}$ using $-i\omega\mathbf{u} = \mathbf{v}$ and the relative fluid-solid displacement $\mathbf{w}$ using $-i\omega\mathbf{w} = \mathbf{q}_1$, Biot's compressibility laws [Equations (9.4) and (9.5)] are exactly recovered, but now with complex effective moduli given by

$$\frac{1}{K_D(\omega)} = a_{11} - \frac{a_{13}^2}{a_{33} - \gamma(\omega)/i\omega}, \tag{9.70}$$

$$B(\omega) = \frac{-a_{12}(a_{33} - \gamma(\omega)/i\omega) + a_{13}(a_{23} + \gamma(\omega)/i\omega)}{(a_{22} - \gamma(\omega)/i\omega)(a_{33} - \gamma(\omega)/i\omega) - (a_{23} + \gamma(\omega)/i\omega)^2}, \tag{9.71}$$

$$\frac{1}{K_U(\omega)} = \frac{1}{K_D(\omega)} + B(\omega)\left(a_{12} - \frac{a_{13}(a_{23} + \gamma(\omega)/i\omega)}{a_{33} - \gamma(\omega)/i\omega}\right). \tag{9.72}$$

The effective complex C and M moduli are obtained from these results using Equations (9.40) and (9.41).

In the three sections that follow, examples of attenuation and dispersion will be presented corresponding to: (1) a double-porosity model of the mesoscopic heterogeneity; (2) a patchy-saturation model of the mesoscopic heterogeneity; and (3) a squirt-flow model of the microcracks in the grains.

9.5.1 DOUBLE POROSITY OR PATCHY SKELETAL PROPERTIES

The mesoscopic heterogeneity in this case is modeled as a mixture of two porous skeletons uniformly saturated by a single fluid.

Various scenarios can be envisioned for how two distinct porosity types might come to reside within a single geological sample. For example, even within an apparently uniform sandstone formation, there can remain a small volume fraction of less-consolidated (even non-cemented) sand grains. This is because diagenesis is a transport process sensitive to even subtle heterogeneity in the initial grain pack, resulting in spatially variable mineral deposition (e.g., Thompson et al.,

1987) and spatially variable skeletal properties. Alternatively, the two porosities might correspond to interwoven lenses of detrital sands and clays; however, any associated anisotropy in the deviatoric seismic response will not be modeled in this chapter. Jointed rock is also reasonably modeled as a double-porosity material. The joints or macroscopic fractures are typically more compressible and have a higher intrinsic permeability than the background host rock they reside within.

The constants a_{ij} in this case are given exactly as (c.f., Berryman and Pride, 2002; Pride and Berryman, 2003a; and Pride et al., 2004)

$$a_{11} = 1/K \tag{9.73}$$

$$a_{22} = \frac{v_1\alpha_1}{K_1}\left(\frac{1}{B_1} - \frac{\alpha_1(1-Q_1)}{1-K_1/K_2}\right) \tag{9.74}$$

$$a_{33} = \frac{v_2\alpha_2}{K_2}\left(\frac{1}{B_2} - \frac{\alpha_2(1-Q_2)}{1-K_2/K_1}\right) \tag{9.75}$$

$$a_{12} = -v_1Q_1\alpha_1/K_1 \tag{9.76}$$

$$a_{13} = -v_2Q_2\alpha_2/K_2 \tag{9.77}$$

$$a_{23} = -\frac{\alpha_1\alpha_2K_1/K_2}{(1-K_1/K_2)^2}\left(\frac{1}{K} - \frac{v_1}{K_1} - \frac{v_2}{K_2}\right) \tag{9.78}$$

where

$$v_1Q_1 = \frac{1-K_2/K}{1-K_2/K_1} \quad \text{and} \quad v_2Q_2 = \frac{1-K_1/K}{1-K_1/K_2}. \tag{9.79}$$

Here, v_i is the volume-fraction of phase i in each averaging volume ($v_1 + v_2 = 1$), K_i is the drained frame modulus of phase i, B_i is the Skempton's coefficient of phase i, and α_i is the Biot-Willis constant of phase i. Models for all of these parameters have been given earlier in Section 9.4.

The one parameter in these a_{ij} that has not yet been modeled is the overall drained modulus $K = 1/a_{11}$ of the two-phase composite. It is through K that all dependence on the mesoscopic geometry of the two phases occurs. As more thoroughly discussed by Pride et al. (2004), a reasonable modeling choice for most geological scenarios in which a more compressible phase 2 is embedded within a stiffer phase 1 is the Hashin and Shtrikman (1963) lower bound given by

$$\frac{1}{K+4G_2/3} = \frac{v_1}{K_1+4G_2/3} + \frac{v_2}{K_2+4G_2/3} \tag{9.80}$$

$$\frac{1}{G+\zeta_2} = \frac{v_1}{G_1+\zeta_2} + \frac{v_2}{G_2+\zeta_2} \tag{9.81}$$

where ζ_2 is defined as

$$\zeta_2 = \frac{G_2}{6}\frac{(9K_2+8G_2)}{(K_2+2G_2)}. \tag{9.82}$$

Roscoe (1973) has shown that this lower bound is exactly realized when the Bruggeman (1935) differential-effective-medium theory is used to model phase 2 as a collection of arbitrarily oriented penny-shaped oblate (squashed) spheroids or disks embedded within a stiffer host phase 1.

When phase 2 is much more permeable than phase 1, the low-frequency limit of the internal transport coefficient γ_o is given by

$$\gamma_o = -\frac{k_1 K_1^d}{\eta L_1^2}\left(\frac{a_{12} + B_o(a_{22} + a_{33})}{R_1 - B_o/B_1}\right)[1 + O(k_1/k_2)]\,. \tag{9.83}$$

where the parameters B_o, R_1, and L_1 are now defined. The dimensionless number B_o is the static Skempton's coefficient for the composite and is exactly

$$B_o = -\frac{(a_{12} + a_{13})}{a_{22} + 2a_{23} + a_{33}}. \tag{9.84}$$

The dimensionless number R_1 is the ratio of the average static confining pressure in the hose phase 1 of a sealed sample divided by the confining pressure applied to the sample and is exactly

$$R_1 = Q_1 + \frac{\alpha_1(1 - Q_1)B_o}{1 - K_1^d/K_2^d} - \frac{v_2}{v_1}\frac{\alpha_2(1 - Q_2)B_o}{1 - K_2^d/K_1^d} \tag{9.85}$$

where the Q_i are given by Equation (9.79). Last, the length L_1 is the distance over which the fluid-pressure gradient still exists in phase 1 in the final approach to fluid-pressure equilibrium and is formally defined as

$$L_1^2 = \frac{1}{V_1}\int_{\Omega_1} \Phi_1\, dV \tag{9.86}$$

where Ω_1 is the region of an averaging volume occupied by phase 1 and having a volume measure V_1. The potential Φ_1 has units of length squared and is a solution of an elliptic boundary-value problem that under conditions where the permeability ratio k_1/k_2 can be considered small, reduces to

$$\nabla^2\Phi_1 = -1 \text{ in } \Omega_1, \tag{9.87}$$

$$\mathbf{n}\cdot\nabla\Phi_1 = 0 \text{ on } \partial E_1, \tag{9.88}$$

$$\Phi_1 = 0 \text{ on } \partial\Omega_{12} \tag{9.89}$$

where $\partial\Omega_{12}$ is the surface separating the two phases within a sample of composite and ∂E_1 is the external surface of the sample that is coincident with phase 1. Pride et al. (2004) suggest values to use for L_1 in various circumstances. For example, if phase 2 is modeled as penny-shaped inclusions of radius a, then $L_1^2 \approx a^2/12$. If it is more appropriate to consider phase 2 as being less permeable than phase 1 (e.g., embedded lenses of clay), then one need only exchange the indices 1 and 2 throughout Equations (9.83)– (9.89) with the exception of B_o, which is independent of permeability.

The transition frequency ω_o corresponds to the onset of a high-frequency regime in which the fluid-pressure-diffusion penetration distance becomes small relative to the scale of the mesoscopic heterogeneity, and is given by

$$\omega_o = \frac{\eta B_1 K_1}{k_1\alpha_1}\left(\gamma_o\frac{V}{S}\right)^2\left(1 + \sqrt{\frac{k_1 B_2 K_2 \alpha_1}{k_2 B_1 K_1 \alpha_2}}\right)^2 \tag{9.90}$$

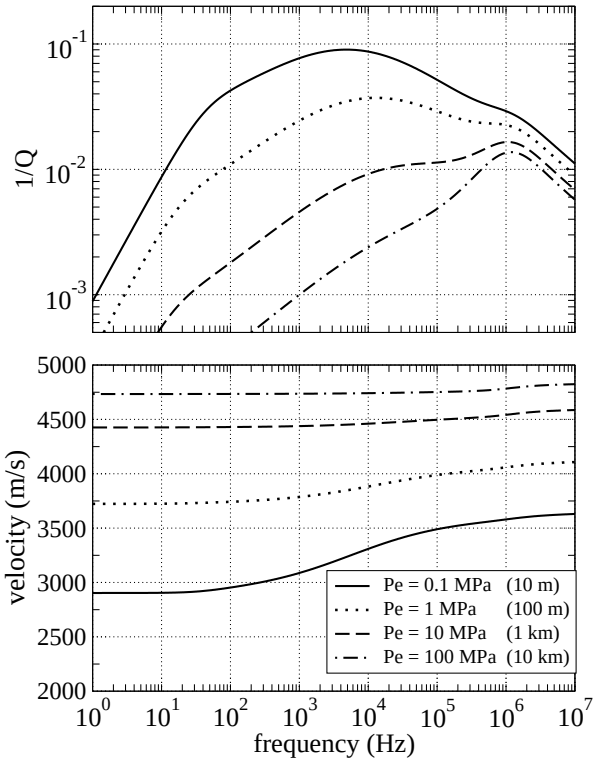

Figure 9.4: The attenuation and phase velocity of compressional waves in the double-porosity model. The thin lenses of phase 2 have frame moduli (K_2 and G_2) modeled using the modified Walton theory given in Section 9.4.3.1 in which both K_2 and G_2 vary strongly with the background effective pressure P_e (or overburden thickness). These lenses of porous continuum 2 are embedded into a phase 1 continuum modeled as a consolidated sandstone.

where S is the surface area of the interface between the two phases in each volume V of composite. For penny-shaped inclusions of phase 2 having radius a, an aspect ratio ϵ and a volume concentration v_2, this volume-to-surface ratio is $V/S = a\epsilon/(2v_2)$.

In Figure 9.4, we give the attenuation and phase determined using the complex slowness of Equation (9.19) and the above complex K_U, C and M moduli. The embedded phase 2 was modeled as 3 cm radius penny-shaped discs having an aspect ratio $\epsilon = 10^{-2}$ and volume concentration of $v_2 = 0.03$. The frame moduli of the embedded spheres were determined using the modified Walton theory of Equation (9.53). These compressible disks of phase 2 are embedded in a consolidated sandstone (phase 1) modeled using Equation (9.54) with $\phi_1 = 0.15$ and $c = 4$. The permeabilities of the two phases are taken as $k_1 = 10^{-14}$ m^2 and $k_2 = 10^{-12}$ m^2. The invariant peak near 10^6 Hz is that caused by the Biot loss (fluid equilibration at the scale of the seismic wavelength) while the principal peak that changes with

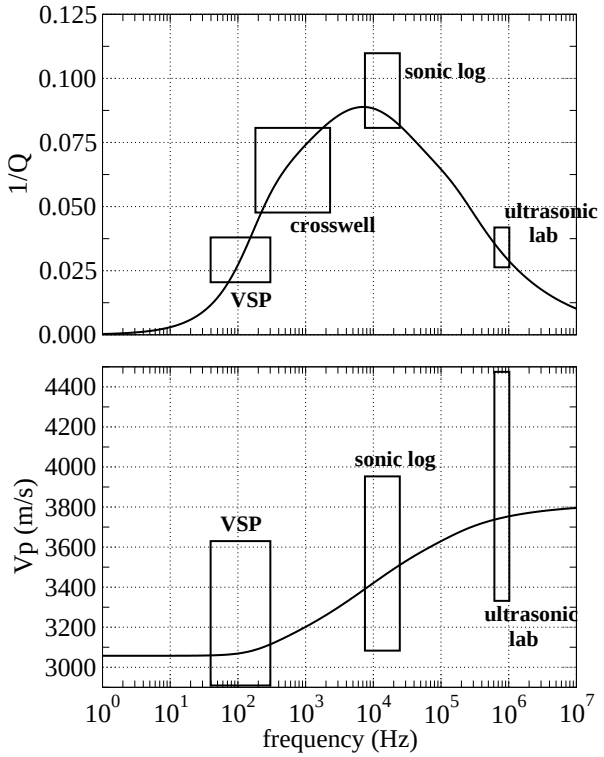

Figure 9.5: Attenuation and dispersion predicted by the double-porosity model (the solid curves) as compared to the data of Sams et al. (1997) [rectangular boxes]. The number of Q^{-1} estimates determined by Sams et al. (1997) falling within each rectangular box are: 40 VSP, 69 crosswell, 854 sonic log and 46 ultrasonic core measurements. A similar number of velocity measurements were made.

P_e is that caused by mesoscopic-scale equilibration. This example demonstrates that the degree of attenuation in the model is controlled principally by the contrast of compressibilities between the two porous phases; the greater the contrast, the greater the mesoscopic fluid-pressure gradient and the greater the mesoscopic flow and attenuation.

In Figure 9.5, we compare the double-porosity model to the data of Sams et al. (1997), who used different seismic measurements (VSP, crosswell, sonic log, and ultrasonic lab) to determine Q^{-1} and P-wave velocity over a wide band of frequencies at their test site in England. The variance of the measurements falling within each rectangular box result from the various rock layers present at this site. Data collection was between four wells that are a few hundred meters deep. The geology at the site is a sequence of layered limestones, sandstones, siltstones, and mudstones. In this example, phase 2 is modeled as unconsolidated penny-shaped inclusions in which $a = 5$ cm (inclusion radius), $\varepsilon = 6 \times 10^{-3}$, $v_2 = 1.2$ %, $k_1 = 80$ mD, $V/S = 1.25$ cm, and $L_1 = 1.45$ cm. The phase 1 host is taken to be a

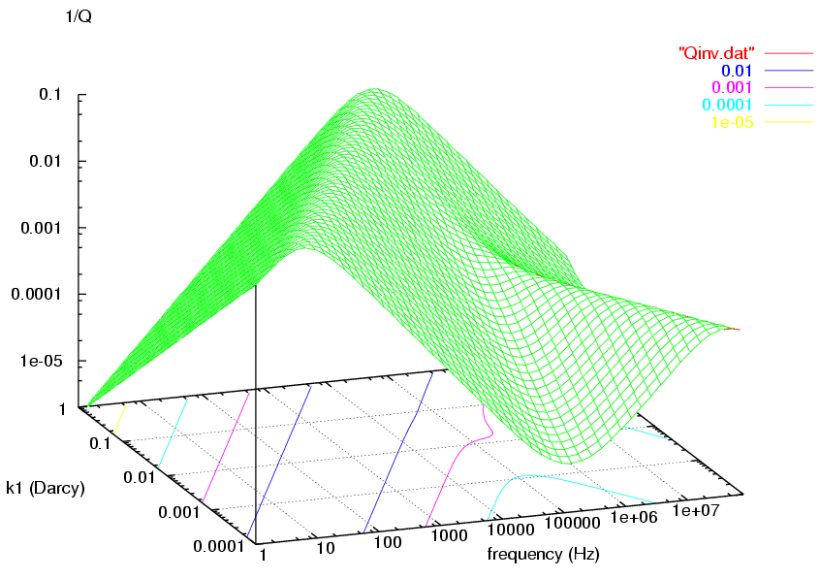

Figure 9.6: The permeability and frequency dependence of the P-wave attenuation in the double-porosity model. The smaller ridge in the attenuation surface between 0.1 and 1 MHz corresponds to the Biot losses. The dominant ridge that has the opposite permeability dependence is the result of mesoscopic flow.

well-consolidated sandstone ($\phi_1 = 0.20$ and $c = 1$).

In Figure 9.6, we allow the permeability k_1 of the host to vary while keeping all other properties fixed (with $P_e = 1$ MPa). The peak value of Q^{-1} is independent of k_1, while the critical frequency at which Q^{-1} is maximum is directly proportional to k_1. Thus the slope $\partial Q^{-1}/\partial\omega$ in the approach to peak attenuation is inversely proportional to k_1. Field measurements of $Q^{-1}(\omega)$ over a range of frequencies could potentially yield information about k_1.

9.5.2 PATCHY SATURATION

All natural hydrological processes by which one fluid non-miscibly invades a region initially occupied by another result in a patchy distribution of the two fluids. The patch sizes are distributed across the entire range of mesoscopic length scales and for many invasion scenarios are expected to be fractal. As a compressional wave squeezes such a material, the patches occupied by the less-compressible fluid will respond with a greater fluid-pressure change than the patches occupied by the more-compressible fluid. The two fluids will then equilibrate by the same type of mesoscopic flow already modeled in the double-porosity model.

Johnson (2001) provides a theory for the complex frequency-dependent undrained bulk modulus in the patchy-saturation model. Alternatively (and equivalently), Pride et al. (2004) provide a patchy-saturation analysis similar to that in the

double-porosity model. This analysis leads to the same effective poroelastic moduli given by Equations (9.70)–(9.72) but with different definitions of the a_{ij} constants and internal transport coefficient $\gamma(\omega)$. In the model, a single uniform porous frame is saturated by patches of fluid 1 and fluid 2. We define porous phase 1 as those regions (patches) occupied by the less mobile fluid and phase 2 as the patches saturated by the more mobile fluid; i.e., by definition $\eta_1 > \eta_2$. This most often (but not necessarily) corresponds to $K_{f1} > K_{f2}$ and to $B_1 > B_2$.

A possible concern in the analysis is whether capillary effects at the local interface separating the two phases need to be allowed for. Tserkovnyak and Johnson (2003) have recently addressed that question in detail. Pride et al. (2004) have demonstrated that the condition for the neglect of surface tension σ on the meniscii separating the two fluids is

$$\frac{\sigma}{k_o K}\frac{V}{S} < 1 \tag{9.91}$$

where S is again the area of the surface separating the two phases in each volume V of composite, k_o is the permeability, and K is the drained bulk modulus taken to be a constant everywhere throughout each sample. As this dimensionless group of terms becomes much larger than one, the meniscii become stiff, and little or no fluid equilibration occurs between the two phases. Accordingly, the attenuation and dispersion vanishes in the limit of very large surface tension. When this inequality is satisfied, the fluids equilibrate under the usual condition that the fluid-pressure changes are continuous across the interface of separation, and there is a correspondingly large amount of attenuation and dispersion. Using the common sandstone values of $k = 100$ mD, $K = 10$ GPa, and $\sigma \approx 10^{-2}$ Pa m, one finds that V/S should be smaller than roughly 10^{-1} m in order to neglect surface tension and capillary effects. This can be considered the more normal situtation in the earth and will be the only situation treated here.

The a_{ij} constants in the patchy saturation model are given by (Pride et al., 2004)

$$a_{11} = 1/K \tag{9.92}$$
$$a_{22} = (-\beta + v_1/B_1)\,\alpha/K \tag{9.93}$$
$$a_{33} = (-\beta + v_2/B_2)\,\alpha/K \tag{9.94}$$
$$a_{12} = -v_1\alpha/K \tag{9.95}$$
$$a_{13} = -v_2\alpha/K \tag{9.96}$$
$$a_{23} = \beta\alpha/K \tag{9.97}$$

where α is the Biot-Willis constant for the material (always independent of fluid type), K is again the drained modulus for the material (also independent of fluid type), and the B_i are the Skempton's coefficients of each patch (all fluid dependence arrives through these terms). Under the assumption that the shear modulus of the material is independent of the fluid type and, accordingly, uniform throughout the patchy-saturation composite, the parameter β is given by

$$\beta = v_1 v_2\left(\frac{v_1}{B_2} + \frac{v_2}{B_1}\right)\left[\frac{\alpha - (1 - K/K_H)/(v_1 B_1 + v_2 B_2)}{\alpha - (1 - K/K_H)(v_1/B_1 + v_2/B_2)}\right]. \tag{9.98}$$

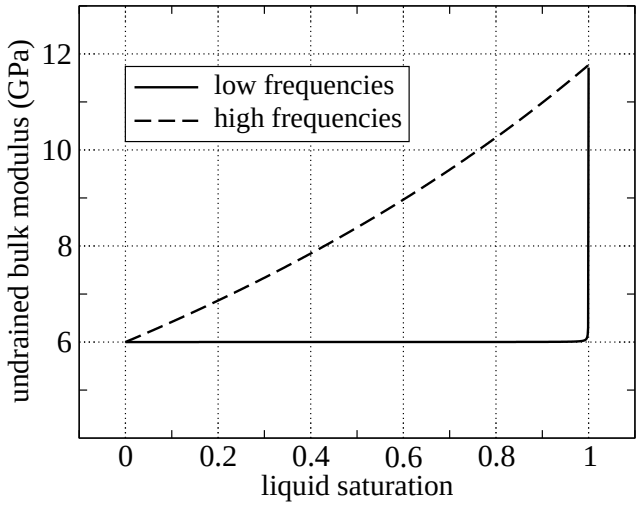

Figure 9.7: The undrained bulk modulus K_U in the limits of low and high frequencies as a function of liquid saturation. The liquid is taken to be water and the gas is air. The properties of the rock correspond to a lightly consolidated sandstone.

The modulus K_H is called the Hill modulus and corresponds to the undrained bulk modulus in the high-frequency limit where no fluid-pressure equilibration has a chance to occur between the two phases [it would also be the undrained bulk modulus at any frequency in the limit of infinite surface tension as defined by the dimensionless group in Equation (9.91)]. It is given by (c.f., Hill, 1963)

$$\frac{1}{K_H + 4G/3} = \frac{v_1}{K/(1-\alpha B_1) + 4G/3} + \frac{v_2}{K/(1-\alpha B_2) + 4G/3} \tag{9.99}$$

where the v_i are again the volume fractions of each phase.

The internal transfer coefficients are given by

$$\gamma_o = \frac{v_1 k_o}{\eta_1 L_1^2}\left[1 + O(\eta_2/\eta_1)\right] \tag{9.100}$$

$$\omega_o = \frac{K B_1}{\eta_1 \alpha}\frac{k_o (v_1 V/S)^2}{L_1^4}\left(1 + \sqrt{\frac{\eta_2 B_2}{\eta_1 B_1}}\right)^2 . \tag{9.101}$$

When the mobility ratio η_2/η_1 can be considered small, the definition of L_1 is again given by Equations (9.86) and (9.89). If phase 2 (the more mobile fluid) is modeled as a sphere of radius a embedded within each larger sphere R of the patchy-saturation composite, then $v_2 = (a/R)^3$, $V/S = a v_2/3$, and $L_1^2 = (9 v_2^{-2/3} a^2/14)(1 - 7 v_2^{1/3}/6)$. These expressions are particularly appropriate when $v_2 \ll v_1$. For other scenarios of the patchy fluid distributions, see Pride et al. (2004) for modeling suggestions.

In the quasi-static limit $\omega/\omega_o \to 0$, the effective Skempton's coefficient B reduces exactly to $1/B = v_1/B_1 + v_2/B_2$. For a Gassmann material (uniform

isotropic grains) this is equivalent to using an effective fluid modulus given by $1/K_f = v_1/K_{f1} + v_2/K_{f2}$ in the Gassmann fluid-substitution relations of Equations (9.43) and (9.44). So in the quasi-static limit, the effective moduli have absolutely no dependence on the geometrical nature of the fluid patches; they depend only on the volume fractions (saturation) of the patches. As already stated, in the opposite limit of very high frequencies, the undrained bulk modulus becomes K_H, which is also independent of the specific shape of the fluid patches. All dependence on the geometry of the patches is restricted to the value of the relaxation frequency separating the high-frequency regime from the low-frequency regime. The relaxation frequency can reside anywhere within the seismic band of frequencies depending on the permeability of the material and the effective patch size. The liquid saturation dependence of the undrained bulk modulus K_U in both the low-frequency and high-frequency limits is shown in Figure 9.7.

9.5.3 SQUIRT FLOW

Laboratory samples of consolidated rock often have broken grain contacts and/or microcracks in the grains. Much of this damage occurs as the rock is brought from depth to the surface. Since diagenetic processes in a sedimentary basin tend to cement microcracks and grain contacts, it is uncertain whether *in situ* rocks have significant numbers of open microcracks. Nonetheless, if such grain-scale damage is present, as it always is in laboratory rock samples at ambient pressures, the fluid-pressure response in the microcracks will be greater than in the principal pore space when the rock is compressed by a P wave. The resulting flow from crack to pore is called "squirt flow," and Dvorkin et al. (1995) have obtained a quantitative model for fully-saturated rocks.

In the squirt model of Dvorkin et al. (1995), the grains of a porous material are themselves allowed to have porosity in the form of microcracks. The effect of each broken grain contact is implicitly taken to be equivalent to a microcrack in a grain. The number of such microcracks per grain is thus limited by the coordination number of the packing and so the total porosity contribution coming from the grains is negligible compared to the porosity of the main pore space.

Pride et al. (2004) have shown that the Dvorkin et al. (1995) squirt model can be analyzed using the double-porosity framework of the previous sections. Phase 1 is now defined to be the pure fluid within the main pore space of a sample and is characterized elastically by the single modulus K_f (fluid bulk modulus). Phase 2 is taken to be the porous (i.e., cracked) grains and characterized by the poroelastic constants K_2 (the drained modulus of an isolated porous grain), α_2 (the Biot-Willis constant of an isolated grain), and B_2 (Skempton's coefficient of an isolated grain) as well as by a permeability k_2. The overall composite of porous grains (phase 2) packed together within the fluid (phase 1) has two distinct properties of its own that must be specified: an overall drained modulus K and an overall permeability k associated with flow through the main pore space. The fraction of each averaging volume occupied by phase 1 is defined to be the "porosity" of the sample $v_1 = \phi$, whereas the volume fraction occupied by the cracked grains is $v_2 = 1 - \phi$ (i.e., the porosity within the grains does not contribute to this definition

of ϕ).

The a_{ij} constants are given exactly by (Pride et al., 2004)

$$a_{11} = 1/K \tag{9.102}$$
$$a_{22} = 1/K - (1+\phi)/K_2 + \phi/K_f \tag{9.103}$$
$$a_{33} = \frac{(1-\phi)\alpha_2}{B_2 K_2} \tag{9.104}$$
$$a_{12} = -1/K + 1/K_2 \tag{9.105}$$
$$a_{13} = -\alpha_2/K_2 \tag{9.106}$$
$$a_{23} = \phi\alpha_2/K_2 \tag{9.107}$$

while the internal transfer coefficients are given by

$$\gamma_o = \frac{(1-\phi)k_2}{\eta L^2} \tag{9.108}$$
$$\omega_o = \frac{B_2 K_2}{\eta\alpha_2}\frac{k_2}{L^2}\left(\frac{(1-\phi)V/S}{L}\right)^2. \tag{9.109}$$

To make predictions, one must propose models for the phase 2 (porous grain) parameters.

If the grains are modeled as spheres of radius R, the fluid-pressure gradient length within the grains can be estimated as $L = R/\sqrt{15}$ and the volume to surface ratio as $V/S = R/[3(1-\phi)]$. The grain porosity is assumed to be in the form of microcracks, so it is natural to define an effective aperture h for these cracks. If the cracks have an average effective radius of R/N_R where N_R is roughly 2 or 3 and if there are on average N_c cracks per grain where N_c is also roughly 2 or 3 then the permeability and porsity of the grains is reasonably modeled as

$$\phi_2 = \frac{3N_c}{4N_R^2}\frac{h}{R} \quad \text{and} \quad k_2 = \phi_2 h^2/12. \tag{9.110}$$

The dimensionless parameters k_2/L^2 and $(1-\phi)(V/S)/L$ required in the expressions for γ_o and ω_o are given by

$$\frac{k_2}{L^2} = \frac{15N_c}{16N_R^2}\left(\frac{h}{R}\right)^3 \quad \text{and} \quad \left(\frac{(1-\phi)V/S}{L}\right)^2 = \frac{5}{3}. \tag{9.111}$$

The normalized fracture aperture h/R is the key parameter in the squirt model.

Pride et al. (2004) have argued that the elastic moduli of the porous grains are reasonably modeled as

$$K_2 = K_s(1-b\phi_2) \tag{9.112}$$
$$\alpha_2 = 1 - K_2/K_s \tag{9.113}$$
$$\frac{1}{B_2} = 1 + \phi_2\frac{K_2}{K_f}\left(\frac{1-K_f/K_s}{1-K_2/K_s}\right) \tag{9.114}$$

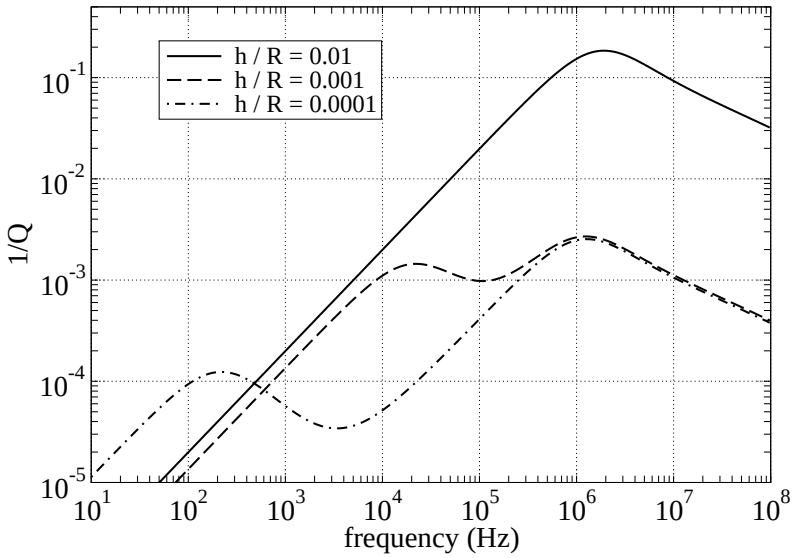

Figure 9.8: The squirt-flow model of P-wave attenuation when the grains are modeled as being spherical of radius R and containing microcracks having effective apertures h. Only the ratio h/R enters the squirt model. The overall drained modulus of the rock corresponds to a consolidated sandstone.

where the parameter b is taken to be independent of h/R and needs to be on the order of 10^2 to explain lab ultrasonic attenuation data. It is true that effective medium theories predict that b should be inversely proportional to the aspect ratio of true open cracks. However, as a crack closes and asperities are brought into contact, there is naturally a decrease in ϕ_2, but there should also be a decrease in b due to the fact that the remaining crack porosity becomes more spherical as new asperities come into contact. Taking b to be constant as crack porosity h/R decreases thus yields a conservative estimate for how the drained modulus increases. The Gassmann fluid-substitution relations were used for α_2 and B_2.

In Figure 9.8 we plot the P-wave attenuation predicted using the above model when the overall drained modulus corresponds to a sandstone [$\phi = 0.2$ and $c = 15$ in Equation (9.54)] having a permeability of 10 mD. For the grain properties, one takes $b = 300$, $N_R = 3$, $N_c = 3$, and $K_s = 37$ GPa (quartz) as fixed constants. The peak in Q^{-1} near 1 MHz that is invariant to h/R is that caused by the macroscopic Biot loss (fluid-pressure equilibration at the scale of the wavelength). The peak that shifts with the square of h/R is that caused by the squirt flow. This figure indicates that although the squirt mechanism is probably operative and perhaps even dominant at ultrasonic frequencies, it does not seem to be involved in explaining the observed levels of intrinsic attenuation in exploration work.

9.6 Discussion and summary

Both equations and guidance have been given for modeling seismic wave speeds and attenuation in isotropic porous materials. A central question that has only been

peripherally answered so far is: Can the permeability of a region be determined if the seismic wave speeds and/or attenuation in that region are known?

The permeability of a rock sample depends on the cross-sectional area ℓ^2 of the smallest pore throat along the flow path that is dominating the fluid transport (the so-called "percolation backbone"). It also depends on the electrical formation factor F, which is the appropriate measure of how tortuous the dominant flow paths are compared to straightline trajectories. Indeed, Thompson et al. (1987) use percolation theory to obtain the law $k = \ell^2/(226F)$ and experimentally demonstrate that this law does an excellent job of predicting rock permeabilities spanning some seven orders of magnitude when ℓ is measured as the breakthrough radius in a mercury porosimetry (invasion) experiment, and when $F = \sigma_{\rm fluid}/\sigma_{\rm rock}$ is obtained by measuring the electrical conductivity σ of the rock and pore fluid. Conceptually, one can change ℓ significantly by placing small amounts of solid (e.g., secondary mineralization) at key points along the percolation backbone without significantly affecting the elastic moduli of the rock. This is sufficient to demonstrate that permeability and seismic velocities are not necessarily linked to each other.

If a connection exists between permeability and seismic velocities, it is related to the case-by-case details of how a rock is built. For example, if secondary mineralization is uniform over the grain surfaces, one could develop a model in which the rock stiffness goes up as the permeability goes down. However, no such model for this presently exists in the literature, and it is known from x-ray tomography and SEM micrographs that secondary mineralization is not uniform, which greatly complicates any such model. As another example, consider unconsolidated sediments. It was shown earlier (Section 9.4.3.1) that grain packs having unimodal grain-size distributions have elastic moduli that are independent of grain size and, therefore, permeability. If smaller radius grains are introduced into the grain packing, one expects a reduction in permeability; however, whether the elastic moduli increase depends on whether these smaller grains form stress-bridging grain-to-grain contacts which in turn depends sensitively to where the smaller grains are positioned in the packing. Statistics for, and even the very definition of (c.f., Torquato, 2000), random grain packs is an open field of research especially when there is a range of grain sizes present.

This discussion is meant to emphasize that although one can imagine scenarios in which permeability and elastic stiffness might both vary as some control knob (like the degree of secondary mineralization or the grain-size distribution) is turned, any such relation depends on the details of how the rock was intially formed and how it has evolved. Perhaps the only thing that can be said with certainty is that no universal relation valid for all rock types can exist between permeability and seismic velocity.

A more promising connection exists between permeability and intrinsic seismic attenuation. It was shown in Sections 9.5.1 and 9.5.2 that mesoscopic heterogeneity is capable of producing the amount of seismic attenuation required to explain the admittedly sparse amount of field data that is available (see Figure 9.5). When a compressional wave squeezes a sample having mesoscopic heterogeneity, the different types of porosity respond with different changes in their fluid pressure. In the type of double-porosity models discussed in Section 9.5, fluid pressure diffuses

from an embedded phase into a host phase, and the permeability of the host phase directly controls the time necessary for equilibration to take place. By observing how Q varies with frequency, one can, in principle, obtain information about the permeability of the host phase in these models. However, inverting seismic data to obtain $Q(\omega)$ over a broad range of frequencies using a single seismic experiment (such as crosswell tomography) is an active point of ongoing research, with no published results presently available.

Note that it is only the permeability of the host phase that affects the frequency dependence of Q in such double-porosity models. If the embedded phase represents disconnected inclusions at small volume fractions, then the host-phase permeability will be controlling both $\partial Q^{-1}/\partial\omega$ and the sample's permeability. However, if the embedded phase represents through-going connected joints or faults, then the host-phase permeability will again be controlling $\partial Q^{-1}/\partial\omega$, but may be unrelated to the sample's permeability, which is being controlled by the through-going joints.

The squirt mechanism presented in Section 9.5.3 has an indirect connection to a sample's permeability. The connection is through the effective size of the grains, which simultaneously affects both the time necessary for the crack porosity to equilibrate with the main pores (the grain size is thus influencing the frequency dependence of Q in the squirt model) and the permeability of the sample. However, it was shown in Section 9.5.3 that squirt is not likely to be operative over the range of frequencies used in seismic exploration.

Arguably the greatest opportunity for connecting permeability to seismic properties is through time-dependent pumping of the fluids in the rock. As the pore pressure changes, Sections 9.4.4 and 9.4.5 show how both the porosity and permeability are changed. The change in seismic velocity is proportional to the change in porosity. Although the percent change in permeability will not, in general, be the same as the percent change in porosity (they have different effective-stress variables), one nonetheless can expect that where seismic velocities change the most, permeability will change the most.

On account of space limitations, anisotropic porous materials were not treated in this chapter. Most earth materials have some degree of anisotropy at the macroscale because of fine layering and/or fracture networks. It is a reasonable postulate that any anisotropic symmetry class determined from seismic measurements must also be satisfied by the permeability tensor. However, no rigorous work along these lines has apparently been published. In his landmark paper, Gassmann (1951) gave the proper fluid-substitution relations that determine how the fluid affects the elastic moduli of an anisotropic porous material. Putting anisotropy into the double-porosity model of mesoscopic and microscopic flow greatly complicates the analysis, since it couples together the response of different tensorial orders within the constitutive laws. So the scalar increment ζ_{int} characterizing fluid transfer between the mesoscopic "patches" becomes coupled to the vectorial Darcy flow, and the average fluid pressure in each patch becomes coupled to the deviatoric (shear) tensor. These complications have not yet been worked through in detail.

On a related note, the possible dispersive nature of the shear modulus was not discussed here. In the presence of local anisotropy (e.g., an embedded fracture or

other elongated local inclusion), an applied shear can result in lobes of compression and dilation surrounding the elongated inclusion. If the material is macroscopically isotropic (e.g., the inclusions or fractures are oriented in all directions), the average fluid pressure will remain zero throughout a sample; however, there will be local regions of enhanced and decreased fluid pressure that result in local fluid flow and an associated shear dispersion and attenuation. These effects have been discussed by Berryman and Wang (2001), and an approximate model has been proposed by Mavko and Jizba (1991); however, no rigorous theory presently exists that accounts for the complex frequency-dependent nature of a rock's shear modulus.

References

Archie, G. E., The electrical resistivity log as an aid in determining some reservoir characteristics, *Trans. AIME*, *146*, 54–62, 1942.

Berge, P. A., H. F. Wang, and B. P. Bonner, Pore-pressure buildup coefficient in synthetic and natural sandstones, *Int. J. Rock Mech. Min. Sci. Geomech. Abstr.*, *30*, 1135–1141, 1993.

Berryman, J. G., Long-wavelength propagation in composite elastic media I. Spherical inclusions, *J. Acoust. Soc. Am.*, *68*, 1809–1819, 1980a.

Berryman, J. G., Long-wavelength propagation in composite elastic media II. Ellipsoidal inclusions, *J. Acoust. Soc. Am.*, *68*, 1820–1831, 1980b.

Berryman, J. G., Effective stress for transport properties of inhomogeneous porous rock, *J. Geophys. Res.*, *97*, 17,409–17,424, 1992.

Berryman, J. G., Mixture theory for rock properties, in *Rock Physics and Phase Relations – A Handbook of Physical Constants*, edited by T. J. Ahrens, Am. Geophys. Union, Washington, DC, 1995.

Berryman, J. G., and S. R. Pride, Models for computing geomechanical constants of double-porosity materials from the constituents' properties, *J. Geophys. Res.*, *107*, 1000–1015, 2002.

Berryman, J. G., and H. F. Wang, The elastic coefficients of double-porosity models for fluid transport in jointed rock, *J. Geophys. Res.*, *100*, 24,611–24,627, 1995.

Berryman, J. G., and H. F. Wang, Dispersion in poroelastic systems, *Phys. Rev. E*, *64*, 011303, 2001.

Biot, M. A., Theory of propagation of elastic waves in a fluid-saturated porous solid. I. Low-frequency range, *J. Acoust. Soc. Am.*, *28*, 168–178, 1956a.

Biot, M. A., Theory of propagation of elastic waves in a fluid-saturated porous solid. II. Higher frequency range, *J. Acoust. Soc. Am.*, *28*, 179–191, 1956b.

Biot, M. A., Mechanics of deformation and acoustic propagation in porous media, *J. Appl. Phys.*, *33*, 1482–1498, 1962.

Biot, M. A., and D. G. Willis, The elastic coefficients of the theory of consolidation, *J. Appl. Mech.*, *24*, 594–601, 1957.

Bruggeman, D. A. G., Berechnung verschiedener physikalischer Konstanten von heterogenen Substanzen, *Ann. Physik. (Leipzig)*, *24*, 636–679, 1935.

Burridge, R., and J. B. Keller, Poroelasticity equations derived from microstructure, *J. Acoust. Soc. Am.*, *70*, 1140–1146, 1981.

Castagna, J. P., M. L. Batzle, and T. K. Kan, Rock physics–the link between rock properties and avo response, in *Offset-Dependent Reflectivity – Theory and Practice of AVO Analysis*, edited by J. P. Castagna and M. M. Backus, Soc. Explor. Geophys., Tulsa, 1993.

Domenico, S. N., Elastic properties of unconsolidated porous reservoirs, *Geophysics*, *42*, 1339–1368, 1977.

Dvorkin, J., G. Mavko, and A. Nur, Squirt flow in fully saturated rocks, *Geophysics*, *60*, 97–107, 1995.

Frenkel, J., On the theory of seismic and seismoelectric phenomena in a moist soil, *J. Physics (Soviet)*, *8*, 230–241, 1944.

Gassmann, F., Über die Elastizität poröser Medien, *Vierteljahrsschrift der Naturforschenden Gesellschaft in Zürich*, *96*, 1–23, 1951.

Gelinsky, S., and S. A. Shapiro, Dynamic-equivalent medium approach for thinly layered saturated sediments, *Geophys. J. Internat.*, *128*, F1–F4, 1997.

Goddard, J. D., Nonlinear elasticity and pressure-dependent wave speeds in granular media, *Proc. R. Soc. Lond. A*, *430*, 105–131, 1990.

Gurevich, B., and S. L. Lopatnikov, Velocity and attenuation of elastic waves in finely layered porous rocks, *Geophys. J. Internat.*, *121*, 933–947, 1995.

Hardin, B. O., and F. E. Richart, Elastic wave velocities in granular soils, *J. Soil Mech. Found. Div. ASCE*, *89*, 33–65, 1963.

Hashin, Z., and S. Shtrikman, A variational approach to the theory of the elastic behavior of multiphase materials, *J. Mech. Phys. Solids*, *11*, 127–140, 1963.

Hill, R., Elastic properties of reinforced solids: Some theoretical principles, *J. Mech. Phys. Solids*, *11*, 357–372, 1963.

Johnson, D. L., Theory of frequency dependent acoustics in patchy-saturated porous media, *J. Acoust. Soc. Am.*, *110*, 682–694, 2001.

Johnson, D. L., J. Koplik, and R. Dashen, Theory of dynamic permeability and tortuosity in fluid-saturated porous media, *J. Fluid Mech.*, *176*, 379–402, 1987.

Korringa, J., R. J. S. Brown, D. D. Thompson, and R. J. Runge, Self-consistent imbedding and the ellipsoidal model for porous rocks, *J. Geophys. Res.*, *84*, 5591–5598, 1979.

Levy, T., Propagation of waves in a fluid-saturated porous elastic solid, *Int. J. Engng. Sci.*, *17*, 1005–1014, 1979.

Mavko, G., and D. Jizba, Estimating grain-scale fluid effects on velocity disperion in rocks, *Geophysics*, *56*, 1940–1949, 1991.

Mavko, G., and A. Nur, Melt squirt in the asthenosphere, *J. Geophys. Res.*, *80*, 1444–1448, 1975.

Mavko, G., and A. Nur, Wave attenuation in partially saturated rocks, *Geophysics*, *44*, 161–178, 1979.

Mavko, G., T. Mukerji, and J. Dvorkin, *The Rock Physics Handbook: Tools for Seismic Analysis in Porous Media*, Cambridge University Press, Cambridge, 1998.

Murphy III, W. F., Effects of microstructure and pore fluids on the acoustic properties of granular sedimentary materials, Ph.D. thesis, Stanford University, Stanford, California, 1982.

Norris, A. N., Low-frequency dispersion and attenuation in partially saturated rocks, *J. Acoust. Soc. Am.*, *94*, 359–370, 1993.

O'Connell, R. J., and B. Budiansky, Viscoelastic properties of fluid-saturated cracked solids, *J. Geophys. Res.*, *82*, 5719–5735, 1977.

Pride, S. R., and J. G. Berryman, Connecting theory to experiment in poroelasticity, *J. Mech. Phys. Solids*, *46*, 719–747, 1998.

Pride, S. R., and J. G. Berryman, Linear dynamics of double-porosity and dual-permeability materials. I. Governing equations and acoustic attenuation, *Phys. Rev. E*, *68*, 036603, 2003a.

Pride, S. R., and J. G. Berryman, Linear dynamics of double-porosity and dual-permeability materials. II. Fluid transport equations, *Phys. Rev. E*, *68*, 036604, 2003b.

Pride, S. R., A. F. Gangi, and F. D. Morgan, Deriving the equations of motion for porous isotropic media, *J. Acoust. Soc. Am.*, *92*, 3278–3290, 1992.

Pride, S. R., J. M. Harris, D. L. Johnson, A. Mateeva, K. T. Nihei, R. L. Nowack, J. W. Rector, H. Spetzler, R. Wu, T. Yamomoto, J. G. Berryman, and M. Fehler, Permeability dependence of seismic amplitudes, *The Leading Edge*, *22*, 518–525, 2003.

Pride, S. R., J. G. Berryman, and J. M. Harris, Seismic attenuation due to wave-induced flow, *J. Geophys. Res.*, *109*, B01201,doi:10.1029/2003JB002639, 2004.

Quan, Y., and J. M. Harris, Seismic attenuation tomography using the frequency shift method, *Geophysics*, *62*, 895–905, 1997.

Roscoe, R., Isotropic composites with elastic or viscoelastic phases: General bounds for the moduli and solutions for special geometries, *Rheologica Acta*, *12*, 404–411, 1973.

Sams, M. S., J. P. Neep, M. H. Worthington, and M. S. King, The measurement of velocity dispersion and frequency-dependent intrinsic attenuation in sedimentary rocks, *Geophysics*, *62*, 1456–1464, 1997.

Sato, H., and M. Fehler, *Seismic wave propagation and scattering in the heterogeneous earth*, Springer-Verlag, New York, 1998.

Skempton, A. W., The pore-pressure coefficients A and B, *Geotechnique*, *4*, 143–147, 1954.

Thompson, A. H., A. J. Katz, and C. E. Krohn, The microgeometry and transport properties of sedimentary rock, *Advances in Physics*, *36*, 625–694, 1987.

Toksoz, M. N., C. H. Cheng, and A. Timur, Velocities of seismic waves in porous rocks, *Geophysics*, *41*, 621–645, 1976.

Torquato, S., T. M. Truskett, and P. G. Debendetti, Is random close packing of spheres well defined?, *Phys. Rev. Lett.*, *84*, 2064–2067, 2000.

Tserkovnyak, Y., and D. L. Johnson, Capillary forces in the acoustics of patchy-saturated porous media, *J. Acoust. Soc. Am.*, *114*, 2596–2606, 2003.

Walton, K., The effective elastic moduli of a random packing of spheres, *J. Mech. Phys. Solids*, *35*, 213–226, 1987.

Wang, H. F., *Theory of Linear Poroelasticity with Applications to Geomechanics and Hydrogeology*, Princeton University Press, Princeton, NJ, 2000.

White, J. E., Computed seismic speeds and attenuation in rocks with partial gas saturation, *Geophysics*, *40*, 224–232, 1975.

White, J. E., N. G. Mikhaylova, and F. M. Lyakhovitsky, Low-frequency seismic waves in fluid-saturated layered rocks, *Izvestija Academy of Sciences USSR, Phys. Solid Earth*, *11*, 654–659, 1975.

Wu, R. S., and K. Aki, Multiple scattering and energy transfer of seismic waves: separation of scattering effect from intrinsic attenuation. II. Application of the theory to Hindu Kush region, *Pure and Applied Geophys.*, *128*, 49–80, 1988.